



Master Thesis

Hydrogen Reduction with Polymer Nanoparticles (Pdots)

Author: Markus Erlacher

Matriculation number: 01506354

Curriculum: UE 066 490

Conducted at

Department of Chemistry - Ångström, Uppsala University

Work carried out

28.08.2022 – 12.1.2023

Report submitted

25.07.2023

Content

Zusammenfassung.....	4
Abstract.....	5
Acknowledgments.....	6
1 Introduction.....	7
1.1 Hydrogen.....	8
1.1.1 Hydrogen as Fuel.....	8
1.1.2 Hydrogen Production Methods	8
1.1.3 Hydrogen Storage.....	9
1.1.4 Safety Concerns	9
1.2 Development of Photocatalysts	10
1.2.1 Natural Photosynthesis	10
1.2.2 Artificial Photosynthesis	12
1.3 Polymer Nanoparticles (Pdots)	14
1.3.1 Preparation of Pdots.....	14
1.3.2 Working Principle	17
1.3.3 State of the Art.....	24
2 Motivation and Aims.....	25
3 Experimental.....	26
3.1 Preparation of Pdots	26
3.1.1 Overview	26
3.1.2 Preparation	26
3.1.3 Struggles in Preparation.....	27
3.2 Analytical Methods.....	28
3.2.1 List of Instruments.....	28
3.2.2 Dynamic Light Scattering.....	28
3.2.3 UV-Vis.....	29
3.2.4 Fluorescence	30
3.2.5 Transient Absorption Spectroscopy (TAS)	32
3.3 Photocatalysis	37

3.3.1 Preparation for photocatalysis	37
3.3.2 Systematic Influences on Photocatalytic Activity.....	38
3.4 Fundamental Experiments.....	39
3.4.1 Quenching Experiments	39
3.4.2 Energy and Charge Transfer Experiments	40
4 Results.....	44
4.1 Confirmation of Preparation	44
4.2 Photocatalytic Results	45
4.3 Mechanistic Studies	47
4.3.1 Possible Pathways.....	47
4.3.2 Absorption and Fluorescence Spectra.....	48
4.3.3 Quenching Experiments	48
4.4.4 Energy and Charge Transfer Studies.....	50
4.4.5 Transient Absorption Spectroscopy (TAS) Studies.....	51
5 Conclusion & Outlook.....	60
Appendix.....	62
References.....	64

Zusammenfassung

Anorganische Katalysatoren zeigen zwar vielversprechende Ergebnisse für die photokatalytische Wasserstofferzeugung, sind aber aufgrund ihrer großen Bandlücke eingeschränkt einsetzbar, so dass nur ein kleiner Teil des Sonnenspektrums für Wasserspaltungsreaktionen genutzt werden kann. Organische Halbleiter hingegen können leicht modifiziert werden, so dass die Bandlücke auf bestimmte Absorptionsbereiche abgestimmt werden kann. Dadurch kann die Anzahl der Photonen, die photokatalytische Reaktionen auslösen können, maximiert werden.

In dieser Arbeit wird ein neues ternäres Polymer-Nanopartikelsystem (Pdots) für die Wasserstoffreduktion in der Photokatalyse vorgestellt. Das System besteht aus dem Polymer PTQ10 und den Akzeptormolekülen ITIC und Y5 und weist eine Wasserstoffentwicklungsrate (HER) von $66,5 \text{ mmol g}^{-1} \text{ h}^{-1}$ oder $1,82 \text{ mL g}^{-1} \text{ h}^{-1}$ auf. Die photophysikalischen Eigenschaften des Systems sowie der einzelnen Komponenten werden mit UV-Vis und Fluoreszenzspektroskopie charakterisiert. Darüber hinaus wird der Einfluss von Energie- und Ladungstransferprozessen zwischen den Komponenten auf die photokatalytische Aktivität mittels stationärer und transientser Absorptionsspektroskopie untersucht. Dabei wird eine Donor/Akzeptor-Grenzfläche zwischen PTQ10 als Donor und ITIC und Y5 als Akzeptoren identifiziert. Die Übertragungsprozesse zwischen Donor und Akzeptor werden von der Energieübertragung dominiert.

Abstract

While inorganic catalysts show promising results for photocatalytic hydrogen production, they are mostly limited due to their large bandgap and therefore, only a small part of the solar spectrum can be utilized for water splitting reactions. Organic semiconductors on the other hand can be easily modified, which allows to tune the band gap to specific absorption regions. This helps maximizing the number of photons that can induce photocatalytic reactions.

This work introduces a new ternary Polymer Nanoparticle (Pdots) system for hydrogen reduction in photocatalysis. The system consists of the polymer PTQ10 and the acceptor molecules ITIC and Y5 and shows a hydrogen evolution rate (HER) of $66.5 \text{ mmol g}^{-1} \text{ h}^{-1}$ or $1.82 \text{ mL g}^{-1} \text{ h}^{-1}$. The photophysical properties of the system as well as the single components is characterized with UV-Vis and Fluorescence Spectroscopy. Furthermore, the impact of energy and charge transfer processes between the components on the photocatalytic activity is investigated using steady state and transient absorption spectroscopy. Thereby, a donor/acceptor interface between PTQ10 as donor, and ITIC and Y5 as acceptors is identified. The transfer processes between donor and acceptor are dominated by energy transfer.

Acknowledgments

First, I would like to thank Haining Tian who introduced me to the fascinating field of Pdots. I really appreciated the discussions and great working environment in his group.

Next, I would like to thank Alexey Cherevan for supervising my thesis at TU Wien and for offering great help during the writing process.

While pursuing a master's project abroad is a wonderful opportunity, it certainly comes with a fair share of challenges. Adapting to a completely new working and social environment is always smoother with the support of others. I am truly thankful to my supervisor Anđela who made this transition so seemingly easy. I will always appreciate her effort and the time she put into this project. I am certain it would not have been possible without her.

I would like to thank my family, especially my brother Johannes and my mum Christa, for their support.

Finally, I extend my heartfelt gratitude to Noa for her exceptional editing skills (a.k.a. Noa GPT). Additionally, I am immensely grateful for her unwavering support, proving that kindness and appreciation know no boundaries, bridging a vast distance of 16,000 km. Thank you, Noa, for being an integral part of this journey.

1 Introduction

Climate change presents one of the biggest challenges in modern history (1, 2). The Intergovernmental Panel on Climate Change (IPCC) predicts drastic consequences if the goal of limiting global warming to 1.5 °C by 2050, compared to pre-industrial levels, cannot be reached (2). In 2015, the global energy demand was estimated to be approximately $1.6 \cdot 10^{14}$ kWh. If no drastic energy saving policies are implemented, by the year 2040, this energy demand is expected to increase by 25 % (3), while the current world population of 8 billion people is still expected to reach 10 billion people in 2050 (4).

The 2015 Paris agreement laid out long-term temperature goals of limiting global warming to well below 2°C, and preferably to below 1.5°C, compared to pre-industrial levels. To achieve the goals of the Paris agreement, a severe reduction of energy consumption in combination with a fast transition to a carbon free industry is needed. This means countries need to invest in and implement renewable energies as soon as possible.

An issue with renewable energies such as wind and solar in comparison to fossil fuels is that they are intermittent, meaning that energy generated is dependent on uncontrollable external factors such as wind speed or amount of sunlight. As such, energy needs to be harvested when available and stored until needed. In addition to traditional energy storage methods like batteries, other methods need to be implemented to address this additional need for storage as renewable energies become more widespread. One of the alternative energy carriers that could address this demand is hydrogen. Even though there are still technological challenges to overcome, hydrogen has become a promising alternative to carbon-based fuels, due to its properties as a non-polluting energy carrier with a high gravimetric energy density (5, 6). However, currently approximately 96 % of hydrogen is produced from fossil fuels (7). Therefore, alternative hydrogen production methods are needed.

The renewable approach to hydrogen production is water splitting. This can either be achieved by electrolysis or through photocatalysis. While water splitting through photocatalysis with inorganic catalysts has already been investigated for some decades, organic catalysts have gained more interest recently, for their properties of smaller bandgaps and the ease to synthesize and adapt them. This way, a larger part of the solar spectrum can be absorbed and thus used for water splitting reactions. For a complete water splitting reaction a complex, concerted redox mechanism is needed. With organic catalysts so far, these reactions were preferably studied separately, with the goal to later implement the reduction and oxidation in a system that allows complete water splitting without sacrificial donors.

This work focuses on the reduction of hydrogen using organic polymer nanoparticles (also known as "Pdots"). Pdots can be easily prepared and have shown promising efficiencies in the past years (8, 9). Finding new combinations of polymers and acceptors for these Pdots and understanding their fundamental photophysical processes is key to further improvement of this method, enabling it to be competitive with other catalysts.

In this work Pdots, consisting of a donor polymer PTQ10 and two acceptors ITIC and Y5 are introduced. Their hydrogen evolution rate (HER) was discussed and photophysical processes were investigated.

1.1 Hydrogen

1.1.1 Hydrogen as Fuel

In the past decades hydrogen has emerged as a promising energy carrier. The simple reaction of hydrogen and oxygen to water can provide the energy either through combustion or more often in electric form through conversion in fuel cells. The only byproduct is water, which is the main selling point, as a closed cycle of converting water to hydrogen and back to water, is rather easy achievable due to the abundancy of water. However, the transition to a (partially) hydrogen-powered world poses significant challenges that must be addressed. To fully comprehend these challenges, a thorough understanding of the properties of hydrogen is necessary.

1.1.2 Hydrogen Production Methods

As of 2017, 96% of hydrogen is still being produced from fossil fuels (7), indicating a pressing need for alternative and renewable hydrogen production methods. In this regard, a few viable methods are briefly outlined below.

Biomass

Plants and trees are naturally grown through the process of natural photosynthesis. Their organic matter can then either be directly burned to use the combustion energy or derive energy carriers, such as ethanol, methanol, and biodiesel. These liquid fuels are the main derivatives of biomass. However, hydrogen can also be obtained from biomass through pyrolysis and steam reforming (10). Biomass is quite controversial, as it can compete with land use in the agricultural sector and can therefore raise food prices or lead to deforestation (11). It is therefore advisable to reduce the use of biomass to certain fields, where competition with food production can be avoided, for example through the use of food waste rather than new crops as a biofuel (12).

Water Electrolysis

Water electrolysis works through cleavage of water using electric energy, which would ideally come from renewable sources. Electrolysis cells can be directly linked to solar cells, wind plants, or hydroelectric plants. The problem of the intermittency of these technologies would therefore be tackled by storing the excessive energy in the form of hydrogen, which could then in return be used to produce electric energy, when demand exceeds supply. (10)

Photochemical Reactions

The linkage of electrolysis cells with other power plants comes with inevitable energy losses. Therefore, the holy grail of hydrogen production would be the direct production of hydrogen from sunlight, through

photocatalysis (10). While this method is still in its early stages, it has recently raised high interest in the scientific community and many different approaches have evolved to establish it. This work focuses on the approach of using polymer nanoparticles (Pdots) as photocatalyst for water splitting reactions. A detailed description of this follows in chapter 1.3.

1.1.3 Hydrogen Storage

Hydrogen is highly reactive and can therefore not be found in its molecular state, but rather bound to other molecules, for example with oxygen in water, or carbon in organic compounds. Therefore, it is not considered an alternative fuel but rather an energy carrier. Next to the production of hydrogen, storage poses a big challenge. While hydrogen has a high gravimetric energy content of 120 MJ kg^{-1} (compared to only 44.4 MJ kg^{-1} for gasoline) (5, 6) in its gaseous form it occupies a large volume, which would require large containers for storage. To address this, researchers have explored various approaches such as pressurizing hydrogen or converting it to its liquid state (13). The choice of hydrogen storage method typically depends on the intended time frame. For short-term storage, liquifying is often preferred due to the higher energy density of hydrogen in its liquid state. However, there is a risk of continuous evaporation and leakage due to the low boiling point of hydrogen. Additionally, special containers are required to maintain the low temperature of -253°C (14, 15). Gas storage is used for large scale storage. Containers for pressurized gas storage are made up of steel, aluminum and carbon fiber reinforced plastic composite materials (16), to omit leaking. A new promising method is solid state storage. The idea is to store hydrogen chemically bound to other materials, which would facilitate both the problem of leakage and the problem of the low volumetric energy density, as hydrogen would appear in a condensed phase. In this case, the main approaches are storage as hydrides with metal alloys and storage in nanomaterials (17-19). Both methods are still in early stages and need further studying to establish the methods commercially.

1.1.4 Safety Concerns

Hydrogen is often perceived as a very dangerous gas, due to its high flammability. Coming back to some of the properties of hydrogen helps to understand the true safety concerns better. Hydrogen has a wide range of flammability, low minimum ignition energy and high burning velocity (20). Furthermore, it has a low boiling point (-253°C) and low ignition temperature (585°C) (21), while it has a large combustion energy (141.6 MJ kg^{-1}), but only little energy is needed to ignite it (0.017 MJ kg^{-1}) (22).

To summarize the safety implications of hydrogen's unique properties, it is important to take certain precautions when handling this substance. Hydrogen's high diffusion rate and ease of ignition make it potentially hazardous, as it can quickly release large amounts of energy. To ensure the safe handling and use of hydrogen, it is important to take appropriate safety measures. This includes using materials with low to no permeability to prevent leaks, as well as implementing sensitive hydrogen detection methods.

To give a context to the safety issues in hydrogen, the University of Miami carried out experiments comparing leakage and ignition of hydrogen fueled cars with gasoline fueled cars. Due to the high diffusion of hydrogen, the fire of the hydrogen fueled car was extinguished after 100 s, leaving the interior of the car unharmed. Meanwhile, the gasoline fueled car kept burning for a long time, due to the slow evaporation of gasoline that kept the fire alive until the whole car was destroyed. (23)

1.2 Development of Photocatalysts

This chapter introduces the concept of using photocatalysts for water splitting. Based on knowledge of natural photosynthesis, presented in sub-chapter 1.2.1, the first semiconductor based artificial photocatalysts were introduced, explained in sub-chapter 1.2.2. This introduction will help with the understanding of the working principle of polymer nanoparticles used in this work. They will be introduced in sub-chapter 1.3.

1.2.1 Natural Photosynthesis

A common approach in research is trying to copy or imitate processes in nature. The same applies to photocatalytic reactions, where systems based on the knowledge of natural photosynthesis are being developed. Therefore, it is vital to understand the basics of natural photosynthesis, in order to better understand the approaches of artificial photocatalytic reactions.

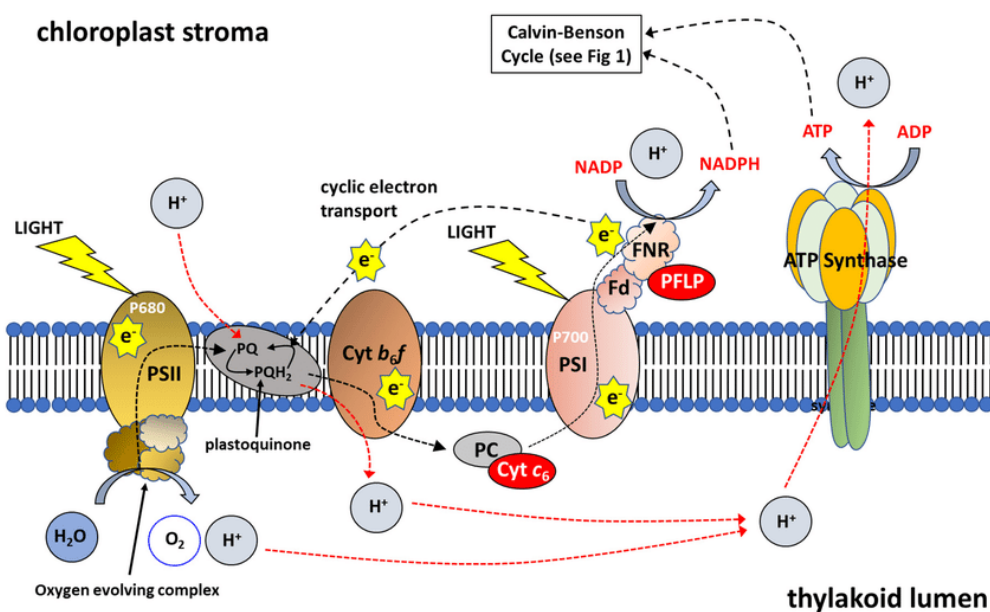


Figure 1: Schematic processes through natural photosynthesis (24)

Figure 1 visualizes the processes of photosynthesis. Since explaining the whole processes would exceed the scope of this work, the focus will remain only on two fundamental steps of natural photosynthesis, that are key for efficient photocatalytic activity in artificial photosynthesis:

1. Light harvesting and energy transfer
2. Charge separation and electron transfer

Light Harvesting and Energy Transfer

Figure 1 illustrates that successful photosynthesis requires several parallel, concerted processes. As such, nature has evolved to use only a few reaction centers (RC), which are surrounded by so called “antenna complexes”. These help to “catch” the energy, which is then transferred to the RC, where the reaction can take place. This raises the probability that the different mechanism can concertedly run to enable the photocatalytic reaction, which splits water.

The antenna complexes are mostly bacteriochlorophylls, chlorophylls, and carotenoids. Once they are excited from incoming sunlight, they transfer their energy to the reaction centers. This energy transfer is thought to happen through Förster Resonance Energy Transfer (FRET), explained more detailed in chapter 1.3.2. However, in reality the transfer mechanism is probably more complex and can be extended with the Redfield Theory (25). Newer studies have shown that quantum coherence also plays a key role in the efficiency of these transfer processes (26).

The main takeaway for artificial photosynthesis is to make use of efficient energy transfer to reaction centers.

Charge Separation and Electron Transfer

Certain limitations apply to the use of photocatalysts for water splitting reactions. The reduction potential of the catalyst needs to be more positive than the water oxidation potential, but more negative than the hydrogen evolution reaction. Nature has addressed this, with a two-step Z-scheme made of two Photosystems, Photosystem I and Photosystem II (PS I & PSII), respectively. The energy scheme of these processes is shown in Figure 2. This scheme enables a better charge separation and one-way electron transfer processes. Furthermore, due to the two-step scheme, a broader spectrum of sunlight can be utilized, since the two steps require smaller energies than the same process with only one PS. The names of the chromophores P680 and P700 refer to the maximum wavelengths for excitation 680 and 700 nm, respectively.

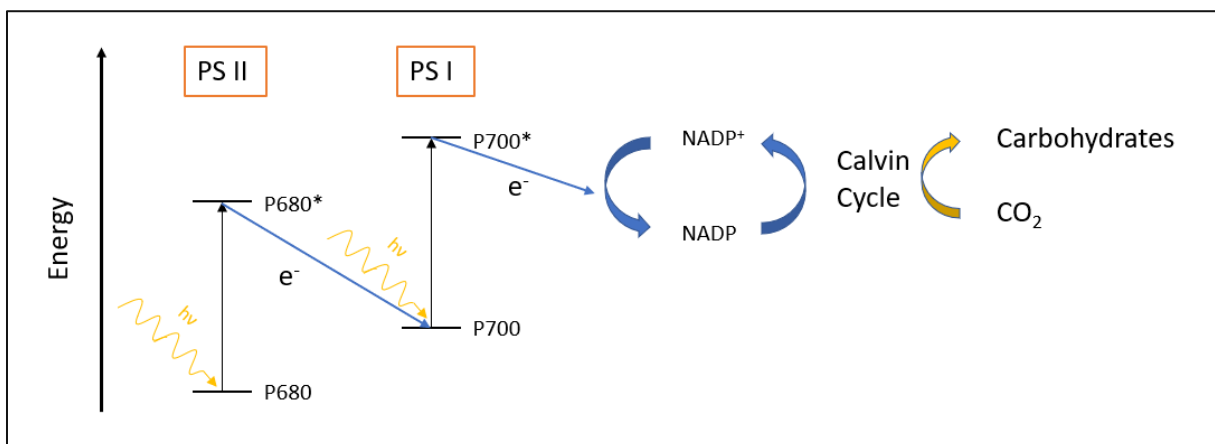


Figure 2: Photosynthesis schematic energy diagram

Efficiency of Photosynthesis

One can calculate the efficiency as follows. The Photosystems PS II and PS I work in series; therefore, two photons are needed for each charge exchange between water and CO_2 . To form dioxygen and reduce CO_2 requires 4 photons, which leads to 8 photons for this process. A glucose molecule $\text{C}_6\text{H}_{12}\text{O}_6$ therefore requires a minimum of 48 photons. To excite P680 a photon with a wavelength smaller than 680 nm is required. 48 photons at this wavelength results in 176 kJ mol^{-1} , which leads to a minimum energy of 8450 kJ mol^{-1} . Burning of glucose in a calorimeter leads to an energy of 2810 kJ mol^{-1} . Therefore, the theoretical efficiency would be about 30 %. However, considering other factors, such as the limited usable amount of sunlight, photodamage and saturation effects, as well as the mechanisms needed to maintain the organization in the plant, this value drops to efficiencies less than 1 % (27).

1.2.2 Artificial Photosynthesis

Natural Photosynthesis offers a greatly sustainable cycle: The same amount of CO_2 that is captured through the growing process of the plants is released again upon combustion. However, this cycle is long, and efficiency is poor, as discussed in the previous sub-chapter. As such, scientists have attempted to replicate natural photosynthesis to make use of the solar energy more efficiently. This artificial approach is generally based on semiconductor physics.

Properties of Semiconductors

The theory of water splitting with inorganic semiconductors has been thoroughly studied, since its first mentioning in 1972 by Fujishima and Honda using a TiO_2 catalyst (28). Semiconductors are materials, which are characterized by their valence band (VB) and conduction band (CB) structure. Unlike metals, where these bands overlap, semiconductors exhibit a band gap between VB and CB, called the energy band gap (E_g), as illustrated in Figure 3. This band gap is a defining characteristic of semiconductor materials, with values typically ranging from 1 to 6 eV. Materials with band gaps larger than 6 eV are classified as insulators.

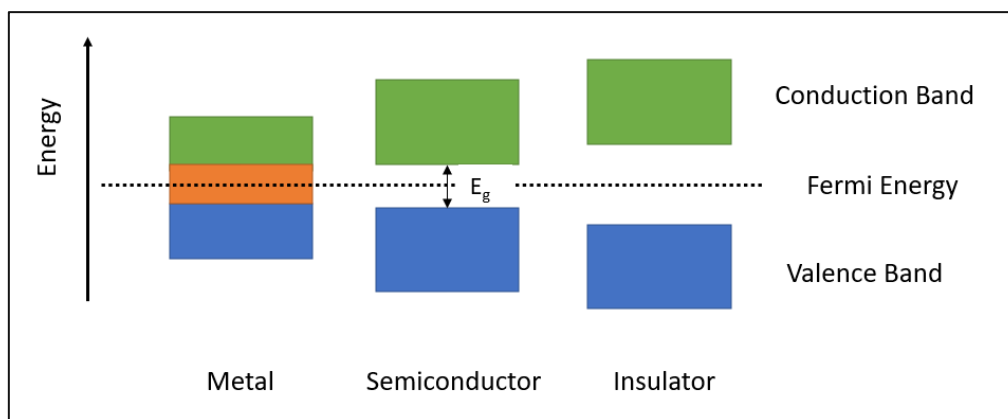


Figure 3: Visualization of the band structure of metals, semiconductors, and insulators

For semiconductors the energy levels between valence band (VB) and conduction band (CB) are forbidden, meaning they are completely unoccupied. For an electron to move from VB to CB, it needs to be excited with energy greater than or equal to E_g . Therefore, E_g determines the spectral range in which electrons can be excited. The energy of photons can be described with:

$$E = h\nu \quad (\text{Eq. 1})$$

where h is Planck's constant and ν the frequency of the excitation wavelength. As shown in this equation, the energy of the photons is directly proportional to their frequency. Therefore, semiconducting materials with large band gaps are only compatible with high frequency light, such as UV. If lower frequency visible light is desired, semiconducting materials with smaller band gaps are required.

Water Splitting Mechanism

The excitation of an electron from VB to CB produces a so-called electron-hole pair (also referred to as "exciton"). Subsequently, the electrons and holes slowly migrate to the surface of the semiconductors where the electron can reduce an acceptor (A) and the hole oxidize a donor (D). This is schematically shown in Figure 4. The water splitting process can be subdivided into a hydrogen evolution reaction (HER) and an oxygen evolution reaction (OER). For the former a potential of 0 eV and for the latter a potential of 1.23 eV (both vs. the normal hydrogen electrode (NHE)) results in a minimum band gap of 1.23 eV, as requirement for semiconducting catalysts. Furthermore, for the reaction to be favorable, the bottom energy state of CB must have a more negative potential than the reduction potential of the H^+/H_2 couple, and the top energy state of VB must be more positive than the oxidation potential of the $\text{H}_2\text{O}/\text{O}_2$ couple. (27, 29)

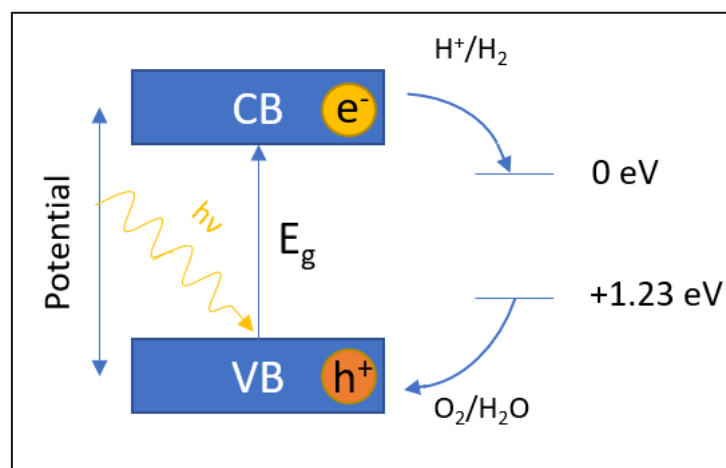


Figure 4: Schematic potential diagram of HER and OER with a semiconductor

The great challenge for water splitting using semiconductors is the large bandgap of common inorganic semiconductors. For example, the band gap of TiO_2 is 3.2 eV, which corresponds to a wavelength of approximately 390 nm. Since only photons with a higher energy can excite electrons to the CB, all

photons in the visible region are inefficient to induce charge separation and therefore the major amount of radiation by the sun cannot be used for water splitting reactions. This problem has been addressed by major research for example by doping semiconductors to tune the band gap to lower energies (27, 30, 31).

Another approach to this problem is the use of organic photocatalysts, which has emerged as a promising alternative to inorganic photocatalysts in recent years. A subgroup of these catalysts are polymer nanoparticles, which will be introduced in the next chapter.

1.3 Polymer Nanoparticles (Pdots)

The first successful organic photocatalyst for water splitting was mentioned in 1985 by Yanagida et al. (32), who was working with poly(p-phenylene) (PPP). However, even with strong efforts and multiple attempts to modify PPP, poor efficiency remained a problem. The first significant breakthrough was not achieved until 2009 with the use of graphitic nitride (33), which remains as one of the most promising organic catalysts to date.

However, other groups of organic photocatalysts have emerged. One of these groups is that of conjugated organic polymers, which are based on Cooper et. al.'s research, who demonstrated the first successful organic photocatalyst systems in 2015 (34). A subgroup of conjugated organic polymers are polymer nanoparticles (also referred to as "Pdots"), which can be used for water splitting reactions as suspended particles in water. The first use of Pdots for water splitting reactions was demonstrated by Tian et al. in 2016 (35).

In this chapter, first the preparation of Pdots will be explained (sub-chapter 1.3.1), followed by an explanation of the photocatalytic working principle (sub-chapter 1.3.2) and finally the state of the art will be presented, highlighting current Pdots efficiencies and approaches (chapter 1.3.3).

1.3.1 Preparation of Pdots

The formation of nanoparticles, in this case Pdots, in water is based on the Ouzo Effect. Following this principle different preparation methods have emerged. The one used in this work is called the nanoprecipitation method.

Ouzo Effect

The Ouzo Effect is named after the Greek alcoholic beverage Ouzo, which contains a certain amount of anis oil. When adding water to Ouzo, this oil will spontaneously nucleate to small stable droplets, thus giving the name to this effect. This can be utilized in photocatalytic systems to form homogeneously distributed nanoparticles in water. The advantages of nanoparticles for photocatalytic reactions are the higher active surface and the shorter diffusion lengths for separated charges, needed to reach the surface of the particles to initiate redox reactions. Both these properties are vital to increase photocatalytic efficiency.

The Ouzo Effect is best explained with a three-component system, consisting of an organic solvent, a co-solvent (usually water) and a solute. First, a diluted solution of the solute in an organic solvent is prepared. Then, it is quickly mixed with an excess amount of water. In a certain region of the three-component diagram (shown in Figure 5), the so called “Ouzo Region”, the solute that shows low solubility in water forms a relatively stable dispersion of small droplets (36).

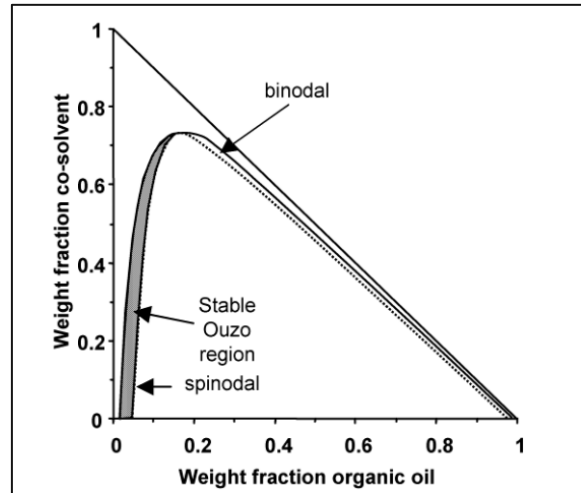


Figure 5: Three component system of an organic solvent, a co-solvent and a solute visualizing the “Ouzo Region”(36).

The effect can further be explained with the metastable region between the binodal and the spinodal region of the three-component system. The binodal line describes the thermodynamical minima of the Gibbs-free-energy as a function of the mole fraction. The spinodal line describes the thermodynamical minima. In case of a high kinetic barrier a system can exist in this metastable region for a long time (36).

A popular model to explain the growth of nanoparticles due to the Ouzo effect is Classical Nucleation Theory (CNT). Hereby, nanoparticles form spontaneously out of the supersaturated solvent, through local concentration fluctuations. The free energy of formation of a nucleus is then described with

$$\Delta G = 4\pi r^2 \gamma + \frac{4}{3} \pi r^3 \Delta g_V \quad (\text{Eq. 2})$$

where r is the radius of the nucleus, γ the surface tension and Δg_V the difference in free energy between the two phases. Since the two terms are of opposite sign, ΔG shows a maximum at a certain nucleus radius r^* with

$$r^* = \frac{-2\gamma}{\Delta g_V} \quad (\text{Eq. 3})$$

For the nanoprecipitation method, mixing of the components needs to be extremely fast, and the nuclei are thought to be formed out of a single batch. Then, nuclei that exceed r^* will grow further by sticking other solutes to it, while nuclei smaller than r^* will dissolve again. The growing of nuclei is limited to

the point where the concentration of the solute has reached thermodynamic equilibrium. (37) Fast mixing of the components has also shown to be vital for uniform size distribution (38, 39).

Another process that can influence particle size and distribution is Ostwald ripening, first introduced in 1961 by Lifschitz and Wagner (40, 41). It describes the growth of larger particles on the expense of smaller ones, leading to a smaller total number of larger particles. (42)

Nanoprecipitation Method

There are different techniques, based on the Ouzo Effect, that allow the implementation of this theory into practice. The mostly used technique, that has also been applied in the following experiments, is the nanoprecipitation method, that was first developed and patented by Fessi et al. in 1989 (43).

As visualized in Figure 6, the nanoprecipitation method requires the use of an organic solvent that is highly miscible with water (e.g., THF, Ethanol...). The components that are planned to be included in the Pdots are first separately dissolved in the organic solvent and then mixed in the desired ratio. The organic mixture is then quickly mixed with water, as shown in the first step in Figure 6. In the next step, the solution is put in an ultrasonic bath, so that the particles are homogenously distributed. Finally, the organic solvent, that should have a lower boiling point than water, is evaporated, through heating or inert gas purging. The concentration of the nanoparticles can further be increased by removing excess amount of water (44).

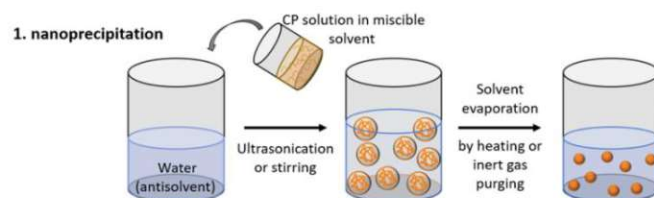


Figure 6: Schematic display of the nanoprecipitation method (45)

However, for homogenous photocatalysis, the insolubility of the polymers in water presents a problem. This can be overcome by adding an amphiphilic co-polymer to the original solution in the organic solvent. With this, the polymers form micelle-like particles, where the polar functional side groups of the co-polymer enable solubility of the nanoparticles in water. Additionally, to the “classic structure” of Pdots, Pt is photodeposited on the surface, before photocatalysis. This was shown to be vital for formation of long-lived charge separated states, through suppressing recombination. A schematic structure of a single component Pdot with photodeposited Pt particles is shown in Figure 7. Orange corresponds to the amphiphilic copolymers, blue to the photocatalytic polymer and black to the cocatalyst Pt.

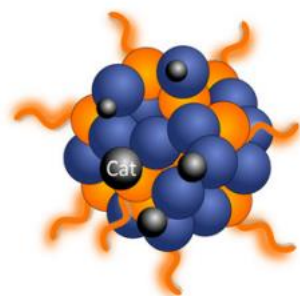


Figure 7: Schematic display of a polymer nanoparticle (pdot) (45)

1.3.2 Working Principle

A solution of nanoparticles in water can serve as catalyst to initiate photocatalytic reactions. These reactions can be triggered by exposure to either artificial light or sunlight and are expected to result in the splitting of water into hydrogen and oxygen. The fundamental theory of the underlying chemical and photophysical processes after irradiation of light are presented here.

Single Component Pdots Photocatalytic Reactions

Water splitting with organic catalysts resembles that of inorganic ones, described in the previous chapter. However, here HOMO and LUMO serve the roles of VB and CB. In Figure 8 an ideal photocatalytic reaction with Pdots is shown. After irradiation with light, exciton formation takes place (step 1). Next, the excitons dissociate to separated charges and are transported to the surface of the nanoparticles (step 2), where the holes and electrons initiate reactions with the help of photodeposited cocatalysts (step 3).

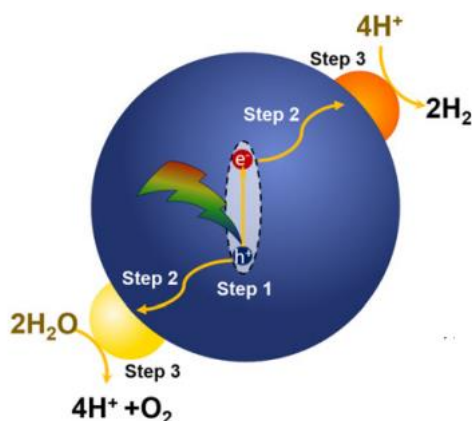


Figure 8: Schematic photocatalytic Pdots reaction (45)

Figure 8 shows a very simplified version of the processes. A more detailed description of four different processes that determine the efficiency of the catalyst follows.

Exciton Formation

After photoexcitation, an electron gets promoted from HOMO to LUMO, forming a coulombically-bound electron-hole pair, also known as exciton. The coulomb attraction V can be described with

$$V = \frac{e^2}{4\pi\epsilon_r\epsilon_0 r} \quad (\text{Eq. 4})$$

where e is the charge of an electron, ϵ_r and ϵ_0 the dielectric constants of the surrounding medium and vacuum, respectively and r the separation distance of electron and hole (46). V needs to be overcome by the exciton within its short lifetime to be able to form long lived charge separated states, which can induce redox reactions. As can be seen in the above formula, V is inversely proportional to the dielectric constant ϵ_r . This explains why charge separation for inorganic photocatalyst happens almost immediately, since TiO_2 shows a very high ϵ_r of 80, while organic molecules used in organic solar cells only show a low ϵ_r of 2 – 4 (47).

One of the strategies to improve charge separation is the introduction of a donor acceptor (D/A) heterojunction, which originates from organic solar cells. (48) The idea is to lead the electron along an energetically downhill path, to improve charge separation. This idea has already been successfully introduced in Pdots photocatalytic reactions (8) and showed improved efficiencies compared to single polymer systems.

Charge carrier transport

To achieve efficient photocatalysis, the dissociated excitons must be successfully transported to the surface of the nanoparticles. While this process is critical for effective energy conversion, the exact mechanism behind it remains largely unknown. However, studies suggest that charge transport mainly occurs through "charge-hopping" (49). Furthermore, it was shown that the addition of Pt can extend the lifetime of charge separation, due to suppressed bimolecular recombination (50), while electron donors like ascorbic acid help to accelerate the decay of separated charges, due to hole transfer to ascorbic acid (45). Both these mechanisms indirectly help to improve charge carrier transport, since this process also depends on the lifetime of the charge separated states.

Electron transport to co-catalyst

On the surface, the charges are transferred to the co catalyst, usually Pt or Pd for hydrogen evolution, where the reaction can take place. Pt has proven to be crucial in enhancing long lived charge separated states by accepting electrons from excited species (8).

Durrant et al. have studied the impact of Pd concentrations in Pdots on quenching of excited states of polymers with Transient Absorption Spectroscopy (51). Increasing the concentration of Pd not only enhanced the efficiency of quenching excited states but also lead to higher efficiencies of hydrogen evolution reaction (HER). The quenching process occurs on ultrashort time frames, typically faster than

200 ps, with some quenching even occurring on a femtosecond time scale. The quenching is thought to be predominantly due to ultrafast electron transfer processes from the excited state of the polymer to the Pd cocatalyst. In the same work, the efficiency of different polymers was compared, and it could be shown that the efficiency is highly dependent on the population of long-lived charges, that a polymer can produce. In conclusion, the efficiency of electron transport to the cocatalyst depends on the concentration of the cocatalyst and the number of long-lived charge-separated states, provided by the polymer.

Exciton Recombination

Exciton recombination is an unwanted process and a major limiting factor for efficient photocatalysis. If the coulomb interaction cannot be overcome, the electron hole pair recombines and emits energy. This process is undesirable, since it is not inducing any redox reactions and is thought to be the main limitation for effective water splitting reactions (9).

Multicomponent Pdots Photocatalytic Reactions

As discussed before, a major problem of Pdots efficiency is poor exciton dissociation. It was shown that the use of multiple polymers and other organic molecules as heterojunction can significantly enhance efficiency due to charge transfer, through energetically downhill processes. This leads to charge separated species, that are more long-living than excitons (8). These heterojunctions can be subdivided into three groups depending on their respective energy levels.

- Type I: Straddling gap
- Type II: Staggered gap
- Type III: Broken gap

The three types are schematically shown in Figure 9.

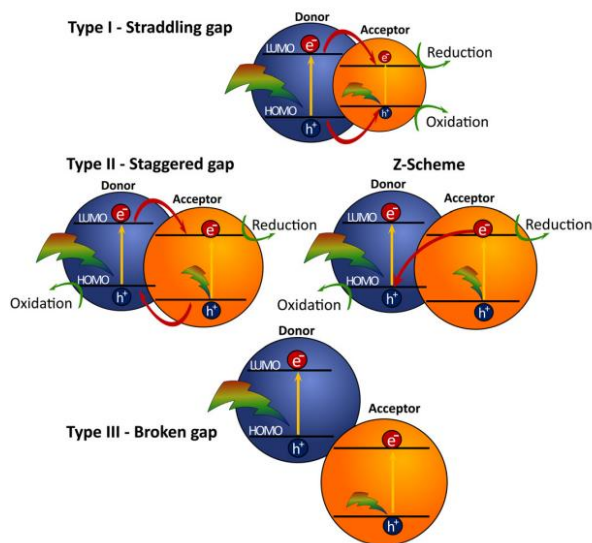


Figure 9: Different types of heterojunctions (45)

The introduction of a heterojunction offers mainly two advantages. The first is the induction of charge transfer processes, electron, and hole transfer, respectively. The second is the use of a broader light spectrum. Since every component only has a limited absorption spectrum, combining several components can enhance the absorption of sunlight, thus increasing the number of photons that can induce reactions. When combining different compounds, they are usually notated as donors (D) and acceptors (A), depending on their role in the system of either donating charges or energy, and accepting charges or energy, respectively. Charge transfer is further subdivided in electron and hole transfer. The processes are schematically shown in Figure 10.

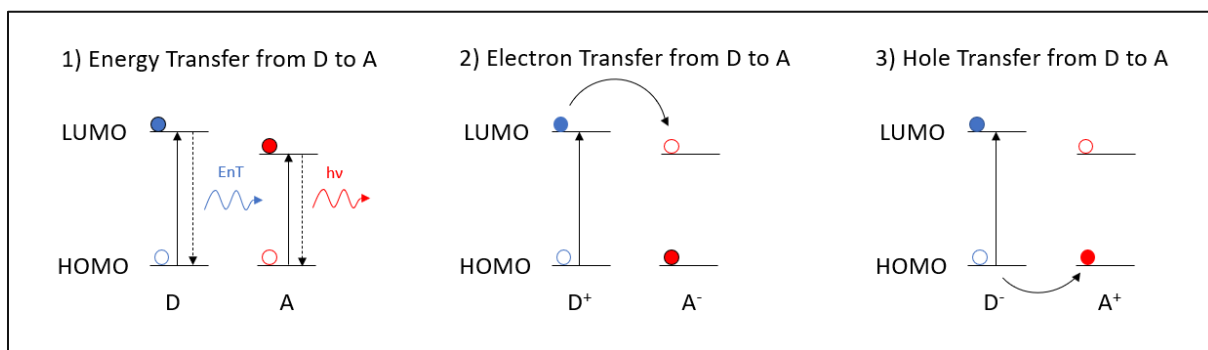


Figure 10: Energy and charge transfer processes in Pdots.

Energy Transfer

The forms of energy transfer related to Pdots mechanisms are Förster Resonance Energy Transfer (FRET) and Dexter-type energy transfer.

- FRET

FRET is a so-called coulombic mechanism, based on dipole-dipole coupling between a donor and acceptor (52, 53). The rate constant of the process is expressed as

$$k_{en}^F = 8.8 \cdot 10^{-25} \frac{K^2 \Phi}{n^4 r_{AB}^6 \tau} J_F \quad (\text{Eq. 5})$$

where K^2 is the orientation factor of the dipoles of the molecules and usually assumed as $K^2 = 2/3$ for random orientation, Φ the luminescence quantum yield, τ the lifetime of the donor in absence of the acceptor, n the solvent refraction index and r_{AB} the distance between donor and acceptor.

J_F is the Förster overlap integral, which, as the name states, describes the amount of overlap between the donor luminescence ($F(\nu)$) and the acceptor's absorption spectrum ($\epsilon(\nu)$), where ν is the frequency of the incoming light.

$$J_F = \frac{\int F(\nu) \frac{\epsilon(\nu)}{\nu^4} d\nu}{\int F(\nu) d\nu} \quad (\text{Eq. 6})$$

The key takeaway from these equations is that the rate is inversely proportional to r^6 , indicating that the transfer mechanism is highly sensitive to distances. This means that even small changes in distance between donor and acceptor have a significant impact on the rate of energy transfer, which is why FRET is also used as a molecular ruler, where the amount of energy transfer can be used to estimate the distance between two molecules. The other takeaway is the direct proportionality to the overlap integral J_F . FRET can only be observed between two molecules if their emission and absorption spectrum strongly overlap (27).

- Dexter

The Dexter-type energy transfer is also referred to as “exchange mechanism”. As the name suggests, energy transfer happens through an exchange of both, an electron and a hole, from donor to acceptor (54). The rate can be described with

$$k_{en}^D = \frac{2\pi}{\hbar} \langle \psi_{A^*B} | \hat{H}^{en} | \psi_{A^*B^*} \rangle^2 J_D \quad (\text{Eq. 7})$$

The electronic coupling between donor and acceptor is described by \hat{H}^{en} , which exhibits an exponential dependence on the distance between the two entities and can be described with

$$\langle \psi_{A^*B} | \hat{H}^{en} | \psi_{A^*B^*} \rangle^2 = H^{en} = H^{en}(0) e^{\left[-\frac{\beta^{en}}{2}(r_{AB}-r_0) \right]} \quad (\text{Eq. 8})$$

The Dexter overlap integral J_D is slightly different to the Förster overlap integral. Here, the normalization is done for both the emission spectrum of the donor as well as the absorption spectrum of the acceptor molecule, which makes J_D independent of the oscillator strengths of both molecules.

$$J_D = \frac{\int F(\nu)\varepsilon(\nu)d\nu}{\int F(\nu)d\nu \int \varepsilon(\nu)d\nu} \quad (\text{Eq. 9})$$

The mechanism can further be described as a double electron transfer. One from LUMO of the donor to LUMO of the acceptor and the other from the HOMO of the acceptor to HOMO of the donor (27). This is shown in Figure 11.

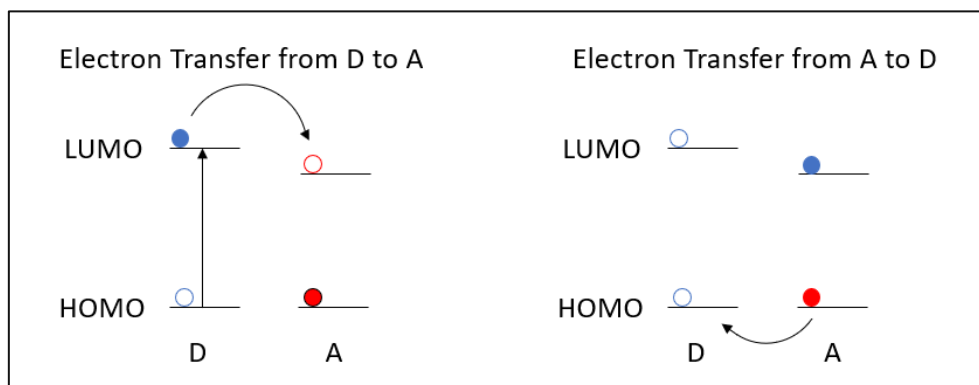


Figure 11: Dexter Mechanism

Electron Transfer

The theory of electron transfer is usually described with Marcus Theory (55, 56). This theory is based on the reorganization of both, inner processes (bonds and atoms) and outer processes (solvent molecules), that take place during an electron transfer. The outer reorganization of the solvent molecules can be well displayed, considering the organization of the polar groups of the solvent. This is shown in Figure 12. While the orientation of the solvent molecules around neutral molecules is random, the orientation around charged molecules is systematic, due to the magnetic interaction between the polar groups with the ions. This reorganization of the solvent molecules requires energy and is therefore notated as “outer reorganization energy”.

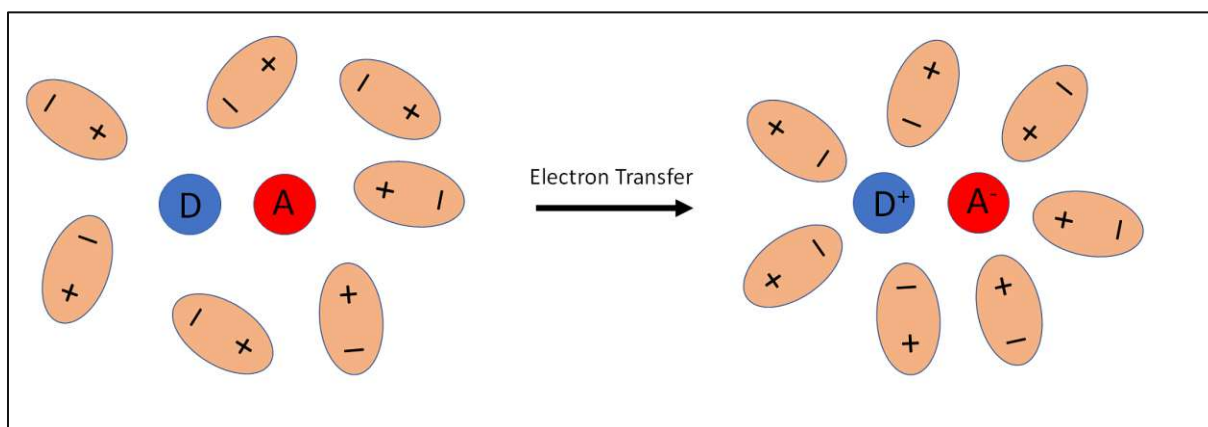


Figure 12: Marcus Theory schematic display of outer reorganization energy.

Mathematically, the reorganization is described with

$$\lambda = \lambda_i + \lambda_o \quad (\text{Eq. 10})$$

where λ_i and λ_o describe the inner and outer reorganization, respectively.

In photochemistry, the reactants and products of a reaction can be represented as potential energy curves. In a two-dimensional representation, these curves can be visualized as parabolic shapes. Electron transfer reactions are depicted using two such curves, representing the initial state (i) and the final state (f) respectively. In the simplest case the curves are of same energy ($\Delta G^0 = 0$), which is shown in Figure 13. The reorganization energy refers to the amount of energy required to reach the potential energy curve of the final state without any movement along the nuclear configuration axis. However, the energetically preferable pathway involves moving along the nuclear configuration axis, where only the free activation energy ΔG^\ddagger must be overcome to enable the reaction to occur.

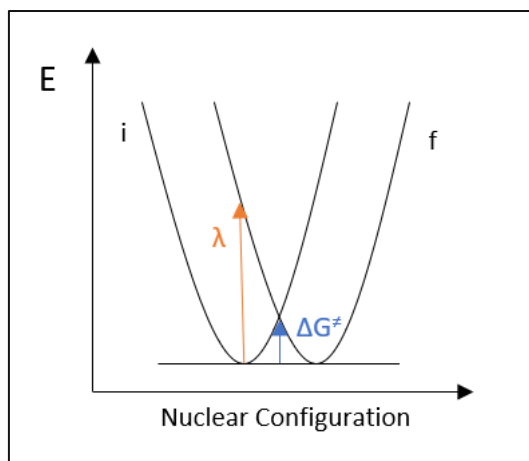


Figure 13: Basic Marcus theory display.

ΔG^\ddagger can be described with

$$\Delta G^\ddagger = \frac{1}{4\lambda}(\Delta G^0 + \lambda)^2 \quad (\text{Eq. 11})$$

Analogously to other kinetic reactions, the activation energy is the key parameter to impact the reaction rate k_{el} that can be described with

$$k_{el} = \nu_N \kappa_{el} e^{-\left(\frac{\Delta G^\ddagger}{RT}\right)} \quad (\text{Eq. 12})$$

where ν_N is the average nuclear frequency factor and κ_{el} is the electronic transmission coefficient.

Figure 13 shows the simplified case where the energies of initial and final state are equal. However, most photocatalytic electron transfer reactions are exergonic, meaning the potential energy curve of the final state is lower in respect to the initial state. In that case one can differentiate between 3 kinetic regimes, shown in Figure 14.

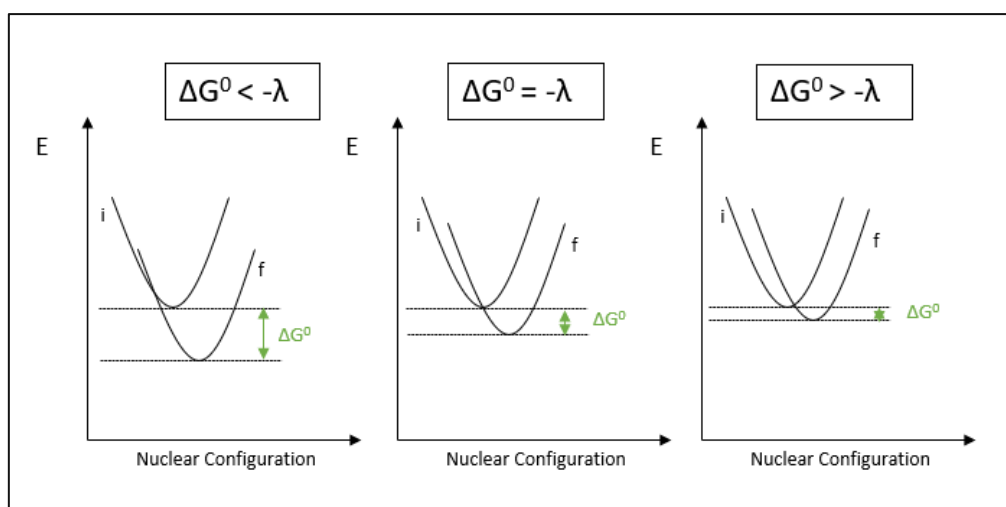


Figure 14: Different exergonic electron transfer processes based on Marcus' theory.

In conventional chemical reactions, the kinetic rate tends to increase the more exergonic the reaction. However, as visualized in Figure 14 for photocatalytic electron transfers, the minimum of the activation energy is reached for $\Delta G^0 = -\lambda$. For processes more exergonic than this, the activation energy increases again, slowing down the kinetics of the reaction according to (Eq. 11) and (Eq. 12).

In conclusion, for electron transfer reactions there is an optimum energy difference of initial and final state, where the activation energy is zero, and therefore, the reaction is most favorable. This region is referred to as the “activationless region”. For reactions with smaller energy differences, the region is called “normal region”. The special case for photocatalytic electron transfer reactions, is that the kinetics decrease again, when the energy difference is too large. This region is referred to as the “inverted region” (27).

1.3.3 State of the Art

The first successful mentioning of a Pdots system for photocatalytic water splitting dates back to 2016 by Tian et al. (35). The polymer poly[(9,9 -dioctylfluorenyl2,7-diy)-co-(1,4-benzo-[2,10 ,3]thiadiazole (PFBT) and polystyrene grafting with carboxyl-group-functionalized ethylene oxide (PS-PEG-COOH) as a copolymer was successfully established in a water reduction system showing HERs of $8.3 \text{ mmol g}^{-1} \text{ h}^{-1}$. The structures of the polymers are shown in Figure 15.

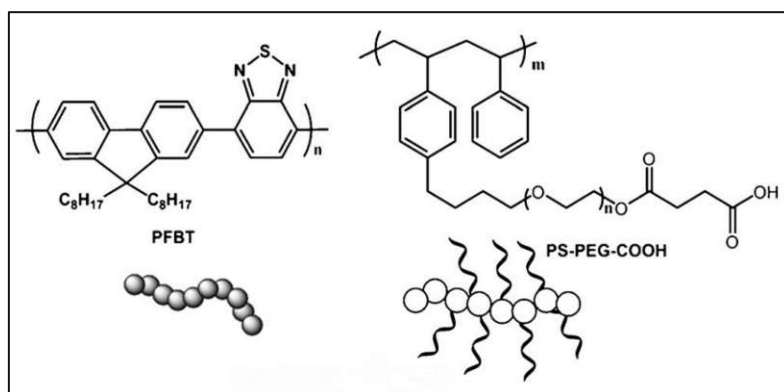


Figure 15: Chemical Structure and schematic steric structure of PFBT and PS-PEG-COOH (35)

Since then, multiple systems with different approaches were published. Currently, many projects work with establishing a heterojunction, with the aim of better charge separation and subsequently higher efficiencies. However, it is difficult to compare systems as the conditions can be very different.

Liu et. al have published a three-component system in 2021 using PFBT, PFODTBT and ITIC. The system showed a HER of $60 \text{ mmol g}^{-1} \text{ h}^{-1}$ or $1.88 \text{ } \mu\text{mole mL}^{-1} \text{ h}^{-1}$ (8). Another ternary system with a remarkable HER of $307 \text{ mmol h}^{-1} \text{ g}^{-1}$ and a maximum apparent quantum efficiency of 5.9 % was published in December 2022 by Yang et al. (57). However, the system of Yang involved the use of 10 wt% of Pt, which is twice as much as that of Liu and the two systems also used different concentrations of pdots, which makes them hardly comparable. In general, this research field is still young, and the focus lies more on fundamental understanding, rather than efficiencies.

2 Motivation and Aims

Organic photocatalysts have been attracting more attention, due to their ease of modification and use of a broader spectrum of the sun. However, to compete with inorganic photocatalysts, the efficiency still needs to be improved. Therefore, it is crucial to explore new systems and study the photophysical processes involved. This information can be utilized to modify polymers and optimize the design of systems to enhance their efficiency. Transient Absorption Spectroscopy (TAS) has been established as a valuable tool for investigating these processes, and when combined with steady-state analytical methods, it can predict the mechanism underlying the water splitting reaction.

In this work a new system consisting of a polymer donor and two acceptor molecules with promising efficiency will be presented and the studies of its photophysical processes discussed. The findings of this research aim to aid in predicting future systems that could further enhance the performance of water splitting.

3 Experimental

3.1 Preparation of Pdots

3.1.1 Overview

The photocatalytic and fundamental studies were performed on combinations of three different components, namely a polymer donor PTQ10, and two organic acceptor molecules ITIC and Y5. It should be noted that the notations “donor” and “acceptor” are based on the originally intended use of the molecules as discussed in the introduction. However, this does not restrict the molecules to their “original roles”, as will be shown in the results. For example, ITIC can function both as donor and acceptor molecule. The structures of the molecules are shown in Figure 16.

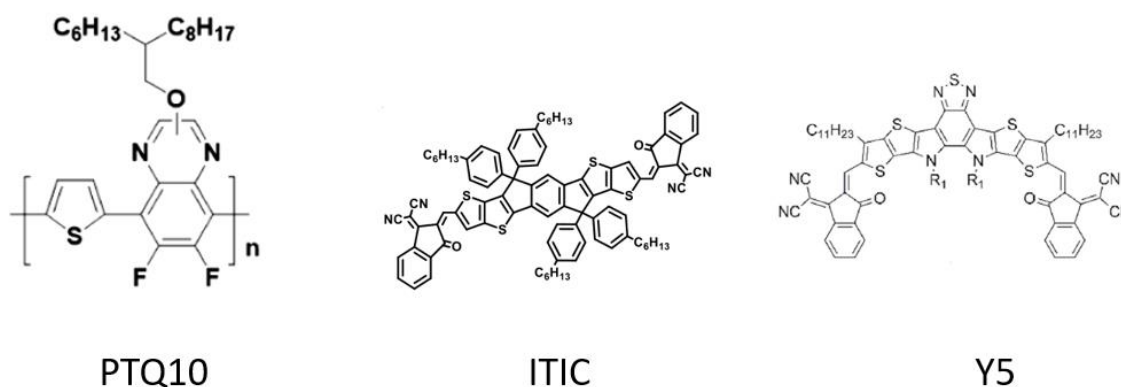


Figure 16: Components used in Pdots (58-60)

For the experiments, different combinations of these components were prepared as Pdots. An overview is shown in Table 1, where they are subdivided into single, binary, and ternary Pdots.

Table 1: List of Pdots prepared for experiments.

Single	Binary	Ternary
PTQ10	PTQ10/ITIC	PTQ10/ITIC/Y5
ITIC	PTQ10/Y5	
Y5	ITIC/Y5	

3.1.2 Preparation

The Pdots used for the following experiments were all prepared using the nanoprecipitation method, described in the introduction. A detailed description of the preparation of the PTQ10/ITIC/Y5 ternary Pdots follows. The preparation of the binary and single Pdots was executed analogously. For all systems the mass ratio of the components to the copolymer (PS-PEG-COOH) was kept constant. Furthermore, for the binary systems, the mass ratio between the two components, compared to the ternary system was kept constant as well.

Preparation of the PTQ10/ITIC/Y5 Ternary Pdots

First, the three components, as well as the copolymer PS-PEG-COOH were each dissolved separately in THF. Then, the solutions were mixed in a certain ratio with a glass pipette. The concentrations, volumes and corresponding mass of each component are shown in Table 2. Depending on the demand, the volumes can be adapted by maintaining ratios.

Table 2: Numbers for preparation of the ternary Pdots

Components	Concentrations (mg mL ⁻¹)	Mass (mg)	Volume (mL)
PTQ10	0.05	0.09	1.8
ITIC	0.1	0.17	1.7
Y5	0.1	0.11	1.1
PS-PEG-COOH	0.5	0.45	0.9

The ternary Pdots THF solution was then sonicated for 1 min. Meanwhile, a beaker filled with 12.5 mL deionized water was heated up to approximately 60 °C. Next, the Pdots THF solution was quickly mixed with the heated water and transferred to a sonic bath, where it was kept for 1 min for thorough mixing. It is important not to keep the solution in the sonic bath for much longer as at some point aggregation will be observed. Afterwards, the solution was transferred to a water bath and heated up to 80 °C for 90 min to evaporate the organic solvent. Since this procedure also evaporates a certain amount of water, the volume of the Pdots solution was reevaluated by transferring it to a new beaker with a glass pipette. Before photocatalysis, these solutions were diluted with water to a **concentration of 34 µg mL⁻¹**.

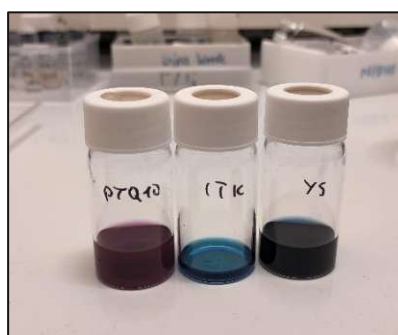


Figure 17: Components solved in THF.

3.1.3 Struggles in Preparation

As discussed on the Ouzo Effect (sub-chapter 1.3.1), it is vital to find the right ratio of solvent (water), antisolvent (THF) and solute (Pdots). For this work there was a limitation to the amount of THF used, due to the solubility of the molecules in THF, as shown in Table 2. Therefore, the easiest way to adapt the preparation is to adapt the amount of water when mixing. Initial attempts at preparing Pdots revealed that concentrations over 200 µg mL⁻¹ often led to strong aggregation. Samples that were affected by this issue are shown in Figure 18.



Figure 18: Aggregation during the preparation of Pdots.

Ideally, the sample should appear as a perfect homogenous solution with a distinct color. This is shown in Figure 19. It was observed that a concentration between 25 and 100 $\mu\text{g mL}^{-1}$ was ideal for successful preparation of the Pdots used in this work.



Figure 19: Pdots under LED light (45).

3.2 Analytical Methods

In this chapter, first the analytical instruments that were used for the experiments are listed. Then, the working principle of the different analytical techniques is discussed.

3.2.1 List of Instruments

Table 3: List of instruments used for Characterization and Photocatalysis.

UV-Vis	Cary 5000 UV-Vis-NIR Spectrophotometer Agilent
Fluorescence (Emission/Excitation)	Fluorolog QM Horiba Scientific
Gas Chromatography	TRACE 1300 Thermo Scientific
Xe Lamp	300 W AULTT CEL-HXF300/CEL-HXUV300

3.2.2 Dynamic Light Scattering

The technique of dynamic light scattering (DLS) measures the Brownian motion of macromolecules in solution, providing information on their size or hydrodynamic radius. The movement of particles is monitored over time, and the diffusion coefficient is obtained by analyzing the intensity fluctuations of scattered light. DLS requires knowledge of accurate temperature, as the viscosity of the solvent affects the Brownian motion of the particles (61).

By monitoring the movement of particles over a period, it is possible to determine the size of macromolecules. Large particles diffuse slowly, resulting in similar positions at different time points, whereas small particles such as solvent molecules move faster and do not adopt a specific position (62).

For a more detailed description of DLS the interested reader is referred to the review listed at (62).

3.2.3 UV-Vis

UV-Vis Spectroscopy is based on the excitation of electrons from the ground state to an excited state. The energy difference between these states is characteristic for molecules and atoms and can therefore be used for characterization.

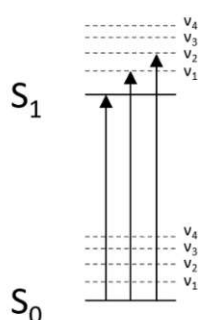


Figure 20: Excitation of electrons in molecules with light from UV-Vis spectrum.

One might expect sharp lines in the spectra representing the characteristic lines. However, while this might be true for atoms it cannot be observed for molecules. Figure 20 shows the energy diagram of a molecule. It consists of different energy states (S_0, S_1, \dots), where each energy state includes several vibrational energy states (v_1, v_2, \dots). Since each vibrational energy state has slightly different energy levels, the result is a group of several different absorptions at slightly different wavelengths. The differences are so small that the spectrometer can usually not resolve them separately, which results in broader absorption bands consisting of different transitions that overlap each other.

Instrumentation

As shown in Figure 21, an UV-Vis Spectrometer consists of a light source, a monochromator, a sample holder, and a detector. First, the light source is split into two beams. One beam enters the reference cell and the other enters the sample cell. The reference cell contains the solvent without analyte (e.g., pure water) and its absorption is subtracted from the absorption of the sample cell, so that only absorption of the analyte remains (63).

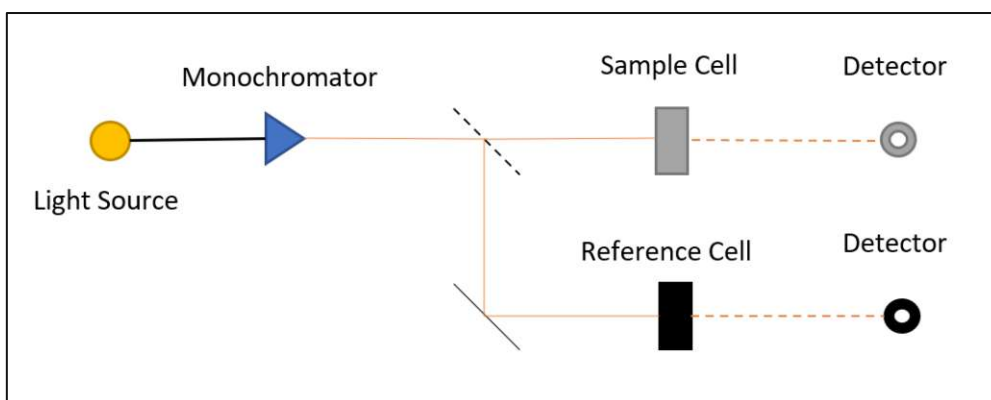


Figure 21: UV-Vis Spectrometer Scheme

3.2.4 Fluorescence

Analogously to UV-Vis Spectroscopy, fluorescence is based on the absorption of light by excitation of electrons from the ground state to a higher energetic state. However, here the following emission through relaxation of the electrons is measured, as visualized in Figure 22. The energy of the photon that is emitted follows a strict energetic behavior based on the energy gap of the analyte. This makes the technique highly characteristic (64).

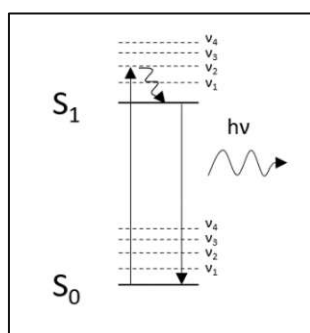


Figure 22: Fluorescence effect.

Stokes Shift

The energy of fluorescent photons is always lower than the energy of the absorbed photons. As shown in Figure 22, every energetic level consists of several vibrational energy states. Through absorption of light, an electron can be excited to different vibrational levels of the respective energetic state. However, the electron will always relax radiationless to the lowest vibrational state before relaxing back to the ground state. Since the energy difference of the lowest vibrational state to the ground state is now smaller, the emitted photon will have a larger wavelength, explaining the red shift of the emission in respect to the absorption (64). This effect is visualized in Figure 23, where the absorption (black) and emission (red) of the acceptor molecule Y5 is shown.

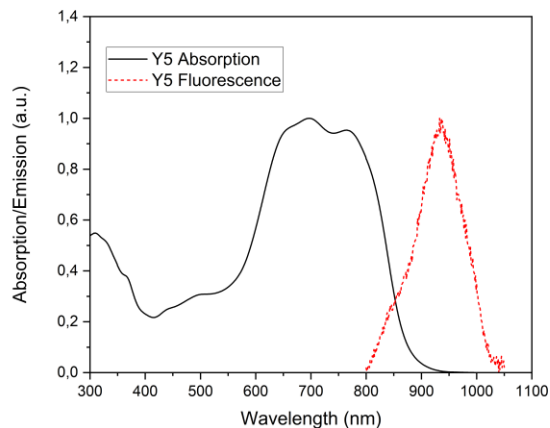


Figure 23: Absorption and Fluorescence of the acceptor molecule Y5, illustrating the red shift.

Kasha's Rule

An important observation to the fluorescence effect is, that the emission spectra are independent from the excitation wavelengths. This is due to Kasha's rule. Based on the principles explained on UV-Vis, there are several energetic levels that the electron can be excited to. That means there are different energies (or wavelengths) that will be absorbed by the molecule. However, with very few exceptions, emission will always come from the first excited energy level to the ground state, because the higher energy levels will quickly dissipate their energy through radiationless transitions down to the lowest vibrational S_1 level where it relaxes to the ground state and releases its characteristic energetical photon, as shown in Figure 22 (64).

Fluorescence Spectrometer

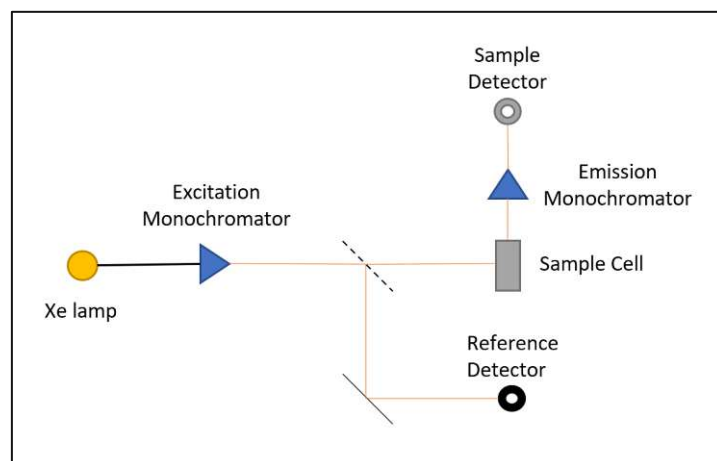


Figure 24: Simplified scheme of a fluorescence spectrometer

Figure 24 shows the principal components of a fluorescence spectrometer. Light passes through the excitation monochromator and is focused on a sample that absorbs part of the light. Then, the sample emits light on the emission monochromator that is placed in a 90° angle in respect to the incident light source, so that only fluorescent light hits the photomultiplier tube (PMT) detector.

There are two types of spectra that can be obtained with a fluorescence spectrometer, namely emission and excitation spectra. When obtaining emission spectra, the excitation monochromator is fixed at a certain wavelength and the emission monochromator is tuned over a chosen wavelength region. Obtaining excitation spectra is exactly contrary. Here, the emission monochromator is fixed at a certain wavelength while the excitation monochromator is tuned over a chosen wavelength region.

Emission spectra can be used to obtain the profile of fluorescence emission of a compound, knowing where it absorbs. The excitation spectra can be used for certain experiments, where it is of interest to see how different excitation wavelengths impact the intensity of fluorescence (64). An example of the use of excitation spectra is shown in sub-chapter 4.4.4.

3.2.5 Transient Absorption Spectroscopy (TAS)

UV/Vis and Fluorescence spectroscopies are powerful tools to investigate steady state energetic properties of samples. However, for photocatalytic reactions time resolved data is vital to study energy and charge transfer reactions. A method to do this is Transient Absorption Spectroscopy (TAS). The advent of ultrafast laser systems has enabled to study photophysical reactions on a fs time scale. The main principles and how this method can be used to interpret mechanistic studies, is explained here.

The instrumental principle of TAS is shown in Figure 25. A pump pulse is used to excite a small number of molecules to an excited state, while the probe laser, overlapping with the pump laser is scanning the absorption with a certain time delay τ . The white light probe is further split into single wavelengths and the signal is analyzed at a diode array detector. Thereby, the pump pulse alternately excites and not excites the sample, resulting in a difference-absorption-spectrum ΔA , that is a function of both wavelength and delay time τ . Note, that the probe laser is significantly lower in intensity, so that its impact on the excitation is negligible (65).

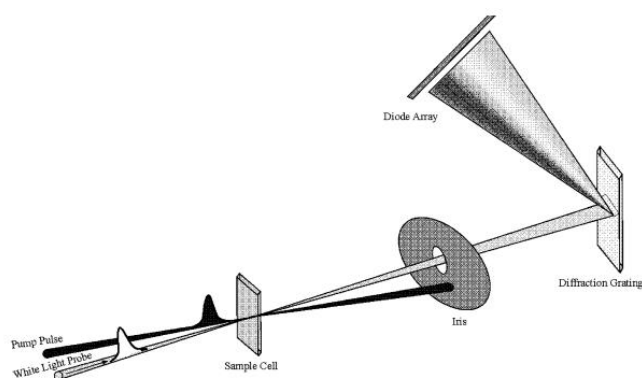


Figure 25: Instrumental Principle of TAS (65).

The resulting signal is a combination of 4 sub signals.

1) Ground State Bleaching (GSB)

The resulting signal is a ΔA signal ($A_2 - A_1$), where A_1 is the absorption of the molecules in their ground state and A_2 the absorption of the molecules after excitation. The absorption signal A_1 resembles the signal of a UV-Vis spectrum. Therefore, the absorption can be derived according to Beer-Lambert from excitation of n molecules in their ground state. After excitation, a certain number m of molecules will transfer to an excited state. For the absorption signal after excitation A_2 , this means the number of molecules in their ground state is now reduced to $n - m$. Again, according to Beer-Lambert the reduction of molecules that absorb at a particular wavelength will lead to a loss in absorption. Therefore, a negative ΔA signal can be observed at the ground state absorption. This phenomenon is called ground state bleaching (GSB) and is schematically shown in Figure 26.

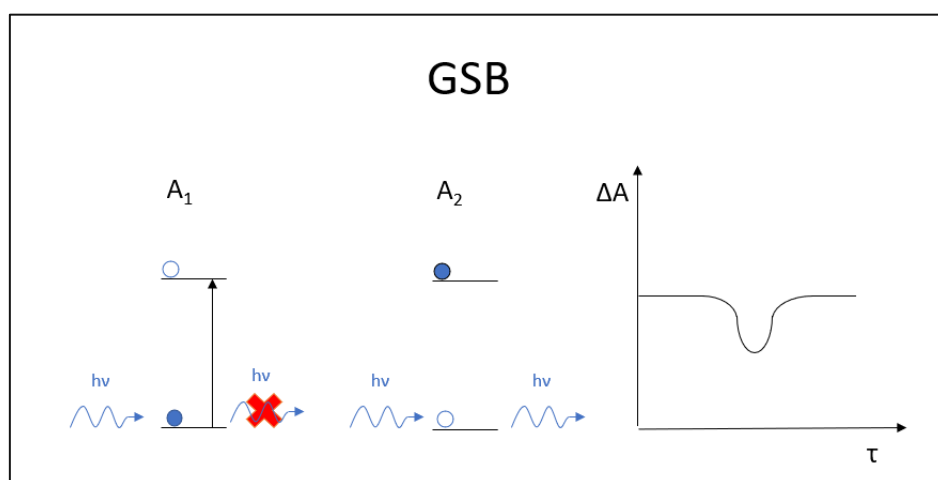


Figure 26: Ground state bleaching in TAS measurements.

2) Stimulated Emission

The principle of stimulated emission (SE) is commonly known from lasers (LASER = **L**ight **A**mplification by **S**timulated **E**mission of **R**adiation). Excited molecules can interfere with the incoming white light where photons with the right frequency cause the excited electron to drop to its ground state, releasing a photon with the same frequency, direction, and polarization as the incoming photon.

For TAS this means that photons that induce SE will double, thus causing a higher signal on the detector at this wavelength. This results in apparent lower absorption and therefore a negative ΔA signal. While GSB follows the principle of UV/Vis absorption signals, SE resembles fluorescence spectra, characteristically Stokes shifted to the ground state absorption. The principle of SE is shown in Figure 27.

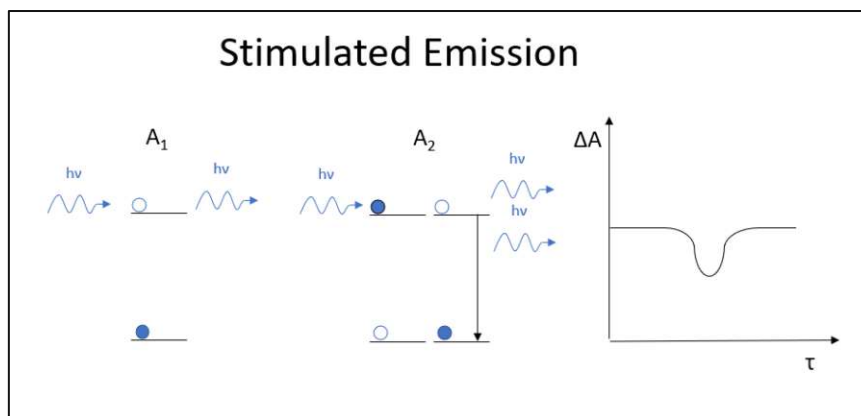


Figure 27: Stimulated Emission in TAS.

3) Excited State Absorption (ESA)

Excited molecules can further be excited to higher energetic states at characteristic wavelengths. Since, in theory, no absorption should be measured at these wavelengths before excitation, ΔA should show positive signals for Excited State Absorption (ESA). These signals are particularly interesting for experiments, as the ΔA signal will decrease continuously in time, and therefore, the lifetime of the excited states can be determined through kinetic studies. The principle of ESA is shown in Figure 28.

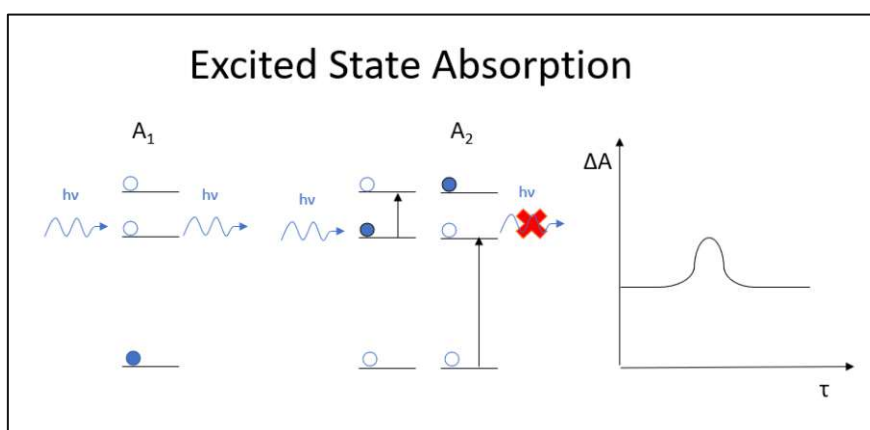


Figure 28: Excited state absorption in TAS.

4) Product Absorption

Finally, excitation of the molecules can lead to reactions, resulting in formation of different states, such as triplet-, charge separated- or isomerized states, which result in a positive ΔA signal for the transient products. After product formation, GSB at the wavelength expected to absorb for this product, can be observed. (65)

3.2.5.1 TAS Setup

An exemplary scheme of a TAS setup is shown in Figure 29.

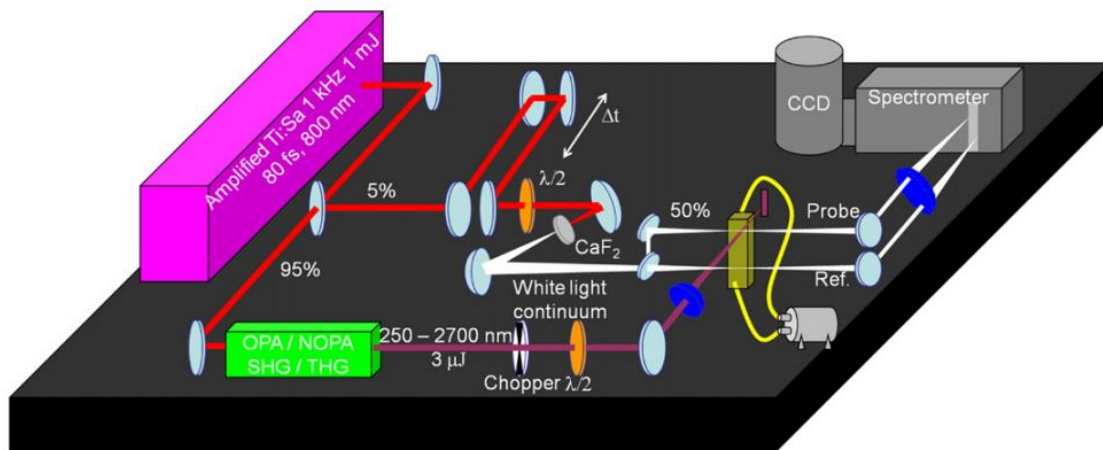


Figure 29: fs-TAS setup (66)

The heart of the system is the optical delay line (delay stage). This is a mechanical setup of multiple mirrors that allow slightly varying the distance of the probe pulse and therefore vary the time delay of the absorption measurement. This setup is placed on a high precision computer-controlled stage. The principle is shown in Figure 30.

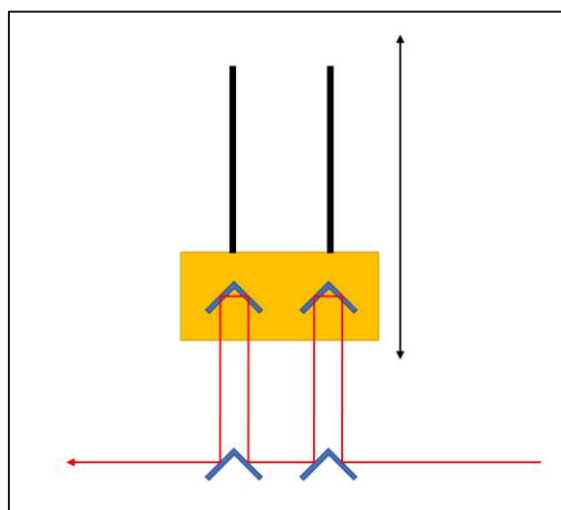


Figure 30: Schematic principle of mirror movement in TAS controlling the measured time delay.

To generate a white light continuum the probe laser is directed at a CaF_2 crystal to create a white light continuum (other crystals like sapphire or MgF_2 can be used as well). Meanwhile, the excitation laser is focused on the probe in a diameter of 130 to 200 μm . To effectively measure the properties of a sample, the probe laser must overlap with the excitation laser, with a slightly smaller diameter. This ensures that the probe laser interacts with the excited sample. While the excitation laser gets blocked after the sample, the probe laser is collimated and directed on a spectrometer. Finally, the computer can generate time resolved ΔA spectra.

To be able to record ΔA spectra, every other pulse of the excitation laser needs to be blocked. This is done by a chopper, which frequency needs to be half the laser pulse frequency. This enables the system to alternately record an absorption spectrum of the non-excited and the excited sample.

$$\Delta A(\lambda) = -\log\left(\frac{I(\lambda)_{pumped}}{I(\lambda)_{unpumped}}\right) \quad (\text{Eq. 13})$$

At the beginning of the measurements, the mirrors on the optical delay path shown in Figure 30 are moved to their starting position. Next, at this time-delay several spectra (usually $10^3 - 10^4$) are recorded to optimize the signal to noise ratio. Then the mirror is moved to the next time delay position to record the next spectra. This procedure is repeated until all desired $\Delta A(\lambda, \tau)$ are recorded. The duration of the measurement depends on the number of time delays and spectra captured per time delay. Typically, acquiring sufficient data for accurate analysis requires several hours per sample.

3.2.5.2 TAS Data Description

The result of the TAS measurements is a large matrix of time correlated absorption data. Figure 31 shows the complete data D on the left side. The goal of data processing is to find the different processes that result in the total data D . This can be done by global analysis. Global analysis helps to identify the rates of these processes. It is based on the equation

$$\Delta A(\lambda, t) = \sum_i A_i(\lambda) e^{-\frac{t}{\tau_i}} \quad (\text{Eq. 14})$$

This equation is also the basis for hard-modelling approaches in this field and the idea is to obtain a weighted sum of exponential decays through computational fitting. The identified exponential decays can then help to understand the underlying processes. However, it is not always an easy task to extract the process mechanism and the physically significant elementary rate constants from the parameters that have been fitted (67).

Another way to describe the data is as a sum of their molar absorption coefficients ϵ_k . This is considered as a soft-modelling method, which shows the separability of wavelength and time and returns qualitative information. It is based on the equation

$$\Delta A(\lambda, t) = \sum_i \epsilon_k(\lambda) C_k(t) l \quad (\text{Eq. 15})$$

where C_k are the respective time related concentrations of the species and l the fixed optical path length. With this equation it is possible to derive a direct description of Beer Lambert's law in matrix notation (66)

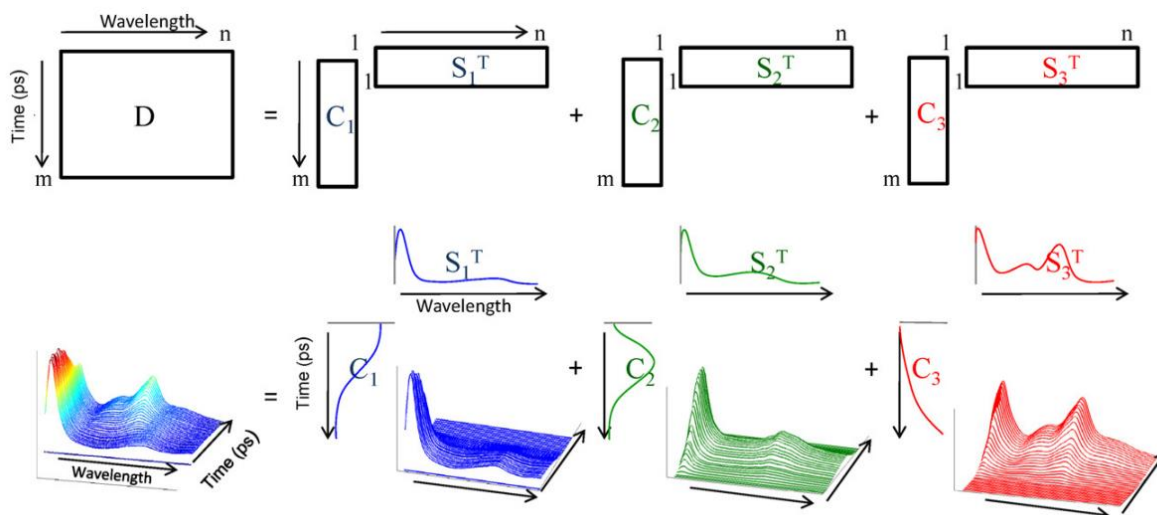


Figure 31: Visualization of TAS data (66)

The Instantaneous Response Function (IRF)

The instantaneous Response Function (or Instrumental Response Function) is the temporal response of the measurement system to the laser pulse. It is usually a Gaussian shaped function, whose width is linked to the time resolution which can be achieved. Another type of information that can be obtained from IRF is the data curvature close to time zero, through group velocity dispersion, which is caused in the crystal that generates the white light continuum. The information of the IRF can help to consider this in preprocessing, and to get valid data for very short time frames (66).

3.3 Photocatalysis

3.3.1 Preparation for photocatalysis

Photocatalysis was performed in 6 mL glass vials. First, 1.5 mL of aqueous Pdots solution with a certain concentration and 20 μL of a 0.04 wt% H_2PtCl_6 solution was added to the vials, which were sealed through crimping. The solution was purged with argon for 30 min to remove oxygen. Additionally, an empty 6 mL vial was purged with argon, for cleaning of the syringes before Gas Chromatography.

Meanwhile, 0.2 M ascorbic acid, that would be used as the sacrificial agent, was prepared, adjusted to pH 4 with 2 M KOH and purged for 10 min with argon. Next, 0.5 mL of the ascorbic acid was added to the Pdots solution.

The headspace of the Pdots solution was purged with argon for another 10 min and then sealed with clay and parafilm to omit leaking of hydrogen and entering of oxygen. Photocatalysis was started by illuminating the samples with a 300 W Xe lamp with an intensity of 1 sun (100 mW cm^{-2}). In certain time steps 100 μL of the headspace of the samples was analyzed on its hydrogen content with gas chromatography.



Figure 32: Purging of photocatalysis samples with argon.

3.3.2 Systematic Influences on Photocatalytic Activity

Up to date there is no official standard on how to perform photocatalytic experiments for Pdots, which brings a problem of comparability to the systems. There are three major influences of system parameters that impact the results of the experiments which will be discussed briefly.

Light Intensity

It is widely accepted to use an intensity of 100 mW cm^{-2} , which is considered to approximately simulate the intensity of the sun. A higher intensity would lead to higher apparent HER, since more photons would interact with the catalyst.

Sacrificial Donor

Sacrificial donors are necessary since the redox reactions of Pdots are studied separately. The choice of donor species and concentration can impact the overall efficiency. The use of a higher concentration and/or lower pH, both lead to higher H^+ concentration, which can increase the apparent efficiency of the catalyst. It was also shown that oxidized ascorbic acid competes with light absorption of the photocatalyst and can therefore slow down the efficiency of the overall system at long term measurements ($> 24 \text{ h}$) (8). However, as all measurements in this work were performed under 10 h, this is expected to play a minor role. As the use of sacrificial donor is only a necessity to be able to study HER, the goal is not to optimize the parameters, but rather stick to parameters published in previous works to enable the results to be comparable. Therefore, in this work 0.2 M ascorbic acid with a pH of 4 was used as sacrificial donor, to achieve similar conditions of a previously published system of Liu et al. (8)

Co-catalyst

In this work Pt was used as co-catalyst. The concentration of co-catalyst is expected to impact the photocatalytic efficiency. However, the aim is to find good working photocatalytic systems that do not rely too heavily on high Pt concentrations. Therefore, in this work the impact of different Pt

concentrations was not investigated. A concentration of 6.9 wt% of Pt was chosen, again to be better comparable to the system of Liu et. al. (8)

3.4 Fundamental Experiments

In this chapter the experimental procedure of the fundamental studies is outlined. The results are shown in chapter 4.3 of this work.

3.4.1 Quenching Experiments

These experiments aim to estimate the amount of quenching of the components in binary systems. First, an excitation wavelength for the different components needs to be chosen. This excitation wavelength should have the least amount of overlap with the absorption of the other component, so that mainly one component gets excited. For ITIC this requires two different excitation wavelengths since it will always either overlap with PTQ10 or Y5. Therefore, the excitation wavelength “ITIC_1” is used for the binary system with Y5 and “ITIC_2” for the binary system with PTQ10. Table 4 shows all the excitation wavelengths chosen for the experiments.

Table 4: Excitation wavelengths for quenching experiments.

Component	Excitation Wavelength (nm)
PTQ10	505
ITIC_1	591
ITIC_2	675
Y5	785

Next, an absorption-emission calibration curve was made for every excitation wavelength, for every component. For this, different concentrations of the same samples were prepared. The absorption at the excitation wavelength of each diluted sample was determined. Then the fluorescence emission of the same samples with the excitation wavelength was measured. The result is a calibration curve, where each data point shows the relation of absorption to emission of a sample. In general, the maximum emission caused by each excitation wavelength was used for the calibration curves. However, for PTQ10 another calibration curve for the experiments with ITIC had to be made, since their maximum emission overlap too much. This calibration curve was produced for emissions at 654 nm. All other calibration curves were performed on the maximum emission wavelength of the respective component.

One of the calibration curves is shown in Figure 33. The other calibration curves can be found in the appendix (Figure 58 to Figure 61).

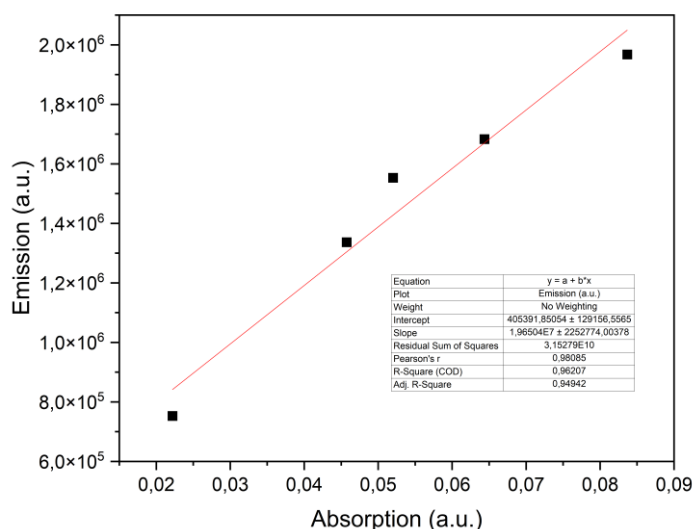


Figure 33: Emission vs Absorption calibration curve of PTQ10 (maximum emission)

Next, for the quenching experiments, dilutions of binary systems whose absorptions were found within the calibration curves were prepared. Then, the absorption at the excitation wavelength was measured, which correlates to an emission value without quenching. However, the real value would be lower due to quenching reactions, for example through energy or charge transfer to other species. The ratio of the actual emission to the emission without quenching returns the quenching value.

$$\text{Quenching} = 1 - \frac{\text{Emission with Quenching}}{\text{Emission without Quenching}} \quad (\text{Eq. 16})$$

3.4.2 Energy and Charge Transfer Experiments

In this chapter a method is presented, showing how one can differentiate between charge and energy transfer, by comparing normalized absorption UV-Vis and fluorescence excitation spectra.

To facilitate the understanding of the method used for binary systems, first the overlapping of absorption and excitation spectra on single systems is explained. This will be shown on the example of the acceptor molecule Y5.

Absorption spectra are quite intuitive. One would see the absorption band at the wavelength region that is specific to that molecule, based on the theory explained in detail in sub-chapter 3.2.4. Fluorescence excitation spectra are however a bit more counterintuitive. To obtain an excitation spectrum, a fixed emission wavelength is chosen. The emission at this wavelength should be at maximum, and not overlap with emission coming from other components. The fixed emission wavelength chosen for Y5 is 934 nm and is shown in Figure 34, indicated with a dashed blue line.

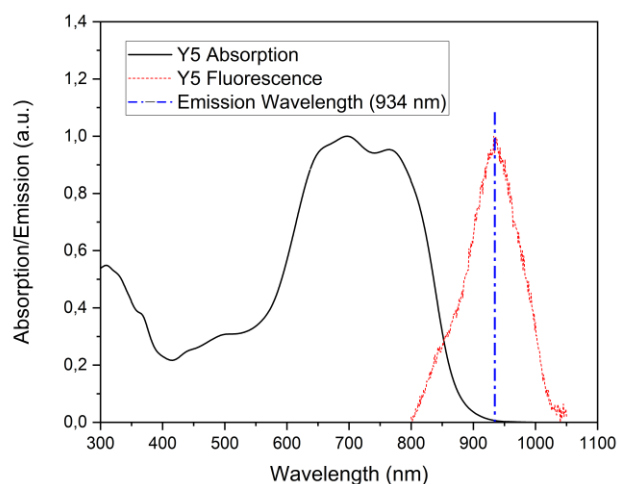


Figure 34: Absorption and Fluorescence Spectra of Y5. The dashed blue line indicates the wavelength at which the excitation spectra will be measured.

Next, the sample is excited at different wavelengths over a certain wavelength region. Each data point in the excitation spectrum thus shows the intensity of fluorescence that follows the excitation at the wavelength of this data point. Since the intensity of fluorescence emission of a molecule is directly proportional to its absorption, the normalized spectra are expected to overlap perfectly, which is shown in Figure 35, again on the example of Y5.

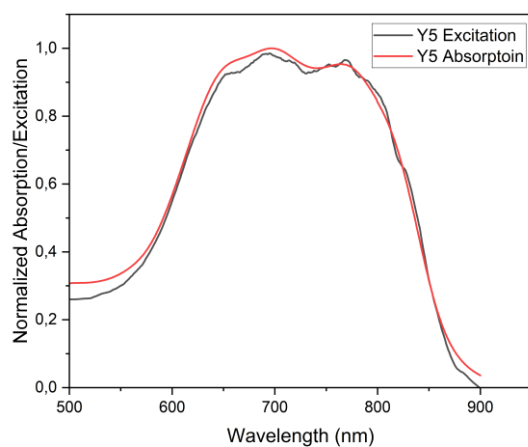


Figure 35: Normalized Absorption and Excitation Spectrum of Y5

For single systems it is apparent that the absorption and excitation spectra need to overlap. However, for multicomponent system it is more complex. This will be explained on the binary system PTQ10/Y5.

To study energy/charge transfer from donor PTQ10 to acceptor Y5, the emission wavelength is set on the maximum emission of Y5 at a wavelength of 934 nm in Figure 36, indicated with a dashed blue line.

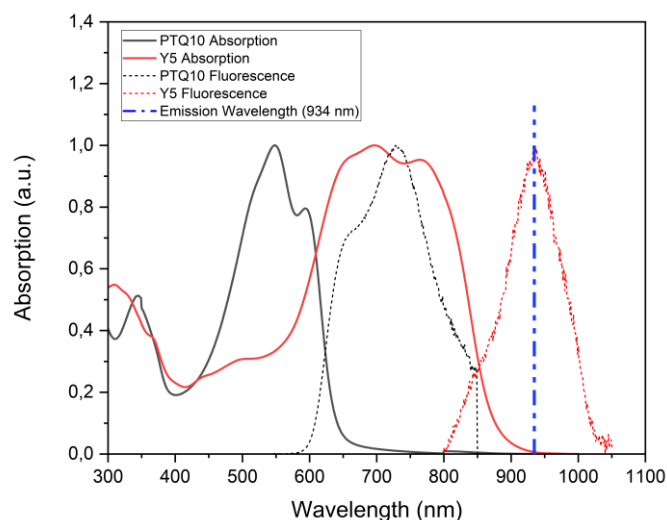


Figure 36: Absorption and Emission Spectra of PTQ10 (black) and Y5 (red). The dashed blue line indicates the emission wavelength chosen for the excitation spectra.

In theory, the absorption spectrum of the binary system is simply a content normalized combination of the absorption of the two single components and independent of any sort of transfer (charge or energy). The excitation spectra at the spectral region, where mainly Y5 absorbs should again overlap with the absorption spectrum, as explained before on the single Y5 example. However, the spectral region where mainly PTQ10 absorbs is expected to differentiate from the absorption spectrum, as the emission from the excited PTQ10 molecules should not contribute to the emission signal, that is set at 934 nm, and therefore outside the emission region of PTQ10. These assumptions are based on no charge/energy transfer from PTQ10 to Y5. However, when considering these transfers, they will in fact impact the excitation spectra, as visualized in Figure 37, where 3 possible scenarios are discussed.

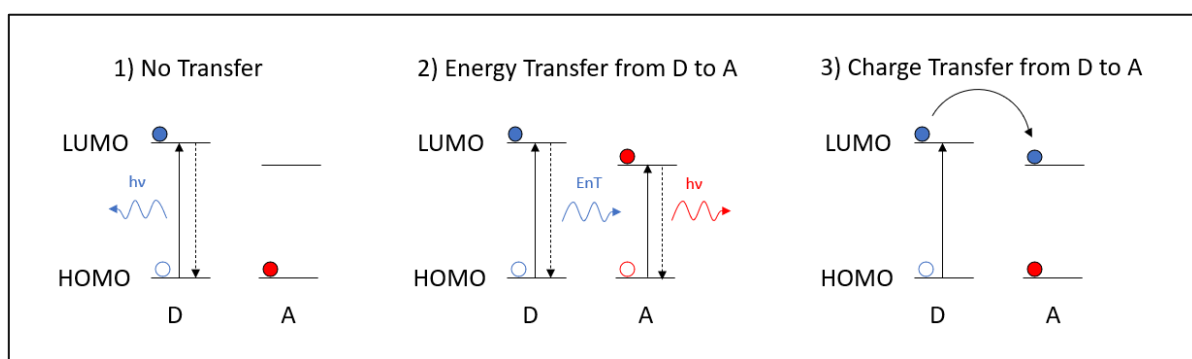


Figure 37: Possible pathways of the donor electron after absorption of light. Donor (D), Acceptor (A)

1) No Transfer

Here the electron simply gets excited and relaxes back to its ground state, emitting characteristic fluorescence light coming from PTQ10. Therefore, this scenario would not contribute to the excitation signal, since the emission of PTQ10 will not be registered by the detector, which is set on a wavelength of 934 nm.

2) Energy Transfer from D to A

In this scenario, the electron relaxes back to its ground state, but instead of emitting a photon, energy gets transferred (Dexter or FRET) to the acceptor molecule and excites an electron from the HOMO to the LUMO. The excited electron relaxes back to its ground state, emitting characteristic fluorescence light. This would contribute to the excitation signal because now the emission comes from the acceptor molecule and therefore gets detected.

3) Charge Transfer from D to A

Here, the donor electron gets excited again, but instead of relaxing to its ground state, the electron gets transferred to the acceptor molecule, reducing it. This does not lead to any emission of light, so it would not contribute to the excitation signal.

In conclusion, only energy transfer from donor to acceptor will contribute to a signal at the absorption region of PTQ10. As shown in Figure 43 the donor molecules in both binary systems (PTQ10/Y5 and ITIC/Y5) were nearly 100 % quenched). This means scenario 1 can be neglected. With the other two scenarios remaining, a complete overlap of absorption and excitation spectra would indicate nearly 100 % of energy transfer, while a “weaker” excitation spectrum would indicate some amount of charge transfer. The results are shown in Figure 44 and Figure 45. This procedure could not be executed on the binary system PTQ10/ITIC, as their emission spectra overlap too strongly (as can be seen in Figure 42), so no distinguished spectra could be obtained.

4 Results

Photocatalysis with organic nanoparticles is a field that is still in its early stages and relies heavily on trial and error. Therefore, it was shown that the most effective method is to first find a working system, and then study the fundamental physical principles. The findings can be used to improve future systems.

This same approach was chosen for this work. As such, the results will be subdivided into three main chapters. The first one will confirm the successful preparation of Pdots. This is followed by the main two chapters. Chapter 4.2 shows the photocatalytic activity of the newly discovered system and chapter 4.3 will discuss the fundamental findings. Eventually, the fundamental findings will be linked to the photocatalytic activities.

4.1 Confirmation of Preparation

An easy method to confirm the successful formation of nanoparticles is Dynamic Light Scattering (DLS). This was done for the ternary Pdots system, and the results are shown in Figure 38.

The particles show a narrow distribution, with most particles ranging from 50 to 150 nm. A small percentage of unwanted aggregates was formed with a diameter of around 5 μm . These could negatively impact the photocatalytic efficiency, since large particles in the μm range are thought to show low hydrogen evolution rates. However, some amount of aggregation cannot be omitted, and a percentage below 1% can be tolerated. Therefore, a successful preparation of nanoparticles can be confirmed.

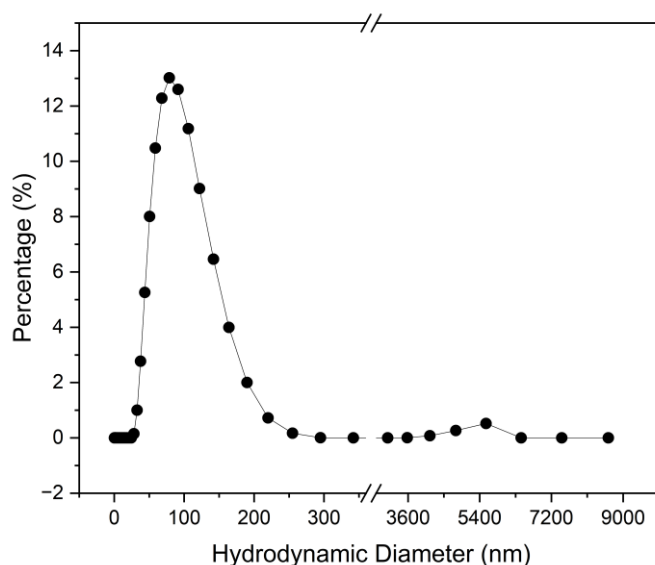


Figure 38: Size distribution of the ternary Pdots PTQ10/ITIC/Y5.

4.2 Photocatalytic Results

The primary goal of the photocatalytic experiments was to determine the efficiency of the ternary system. However, it can also be of interest to study the efficiency of all binary and single subgroups, of the components used in the ternary system. Thereby, to make it comparable, their mass ratios were kept the same, and adapted to the same concentration ($34 \mu\text{g mL}^{-1}$). The results are shown in Figure 39.

It must be stated that, for time consuming reasons, photocatalysis was only performed once for every sample. Therefore, no error bars can be seen in Figure 39, and thus the graph should help to identify certain trends rather than show exact Hydrogen Evolution Rates (HER).

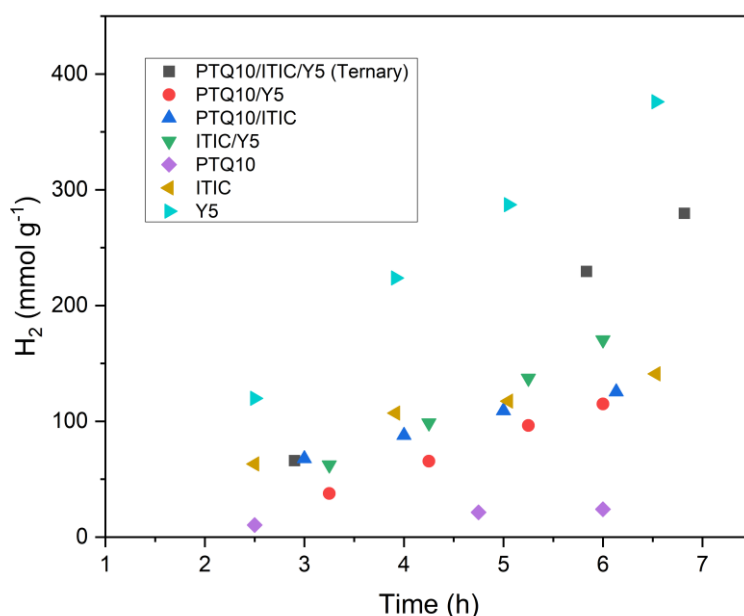


Figure 39: Comparison of Photocatalytic performance of all possible combinations of the three components used.

The single donor polymer PTQ10 (purple) performs exceptionally bad, compared to all other samples. As discussed before, single polymer nanoparticles tend to perform worse than multicomponent ones, mainly due to poor exciton dissociation. Introducing a heterojunction with other components with different energy levels can enable charge separation, and thus better HER. The binary versions of PTQ10 with ITIC (dark blue) and Y5 (red) performed better multifold.

Next, the single nanoparticles of ITIC (yellow) and Y5 (turquoise) perform surprisingly well even without other components that could help with charge separation. In particular, Y5 even outperformed the ternary system. Therefore, arguably the better performance of the binary systems PTQ10/ITIC and PTQ10/Y5 could also come from the fantastic photocatalytic efficiency of the acceptor molecules ITIC and Y5. This can be further investigated in the quenching experiments that follow in the next chapters. If PTQ10 exhibits a high level of quenching, it could suggest that it is indeed involved in the

photocatalytic activity. Furthermore, the roles of energy and charge transfer need to be further investigated. A dominance in energy transfer would indicate that PTQ10 would rather work as an “antenna” that absorbs energy in a region where the acceptor cannot absorb, and then transfers its energy to the acceptor molecule, which dominates the photocatalytic reaction. A contribution of charge transfer however would indicate a more active role of PTQ10 in the photocatalytic process. Either way, the fact that the ternary system outperforms the binary system of ITIC/Y5 indicates that PTQ10 does in fact contribute to the overall photocatalytic efficiency.

However, the implementation of a ternary system is only viable if it outperforms all its subgroups, otherwise the use of more components than necessary would be counterproductive. It can be expected that the efficiency also depends on the ratios of the components. Therefore, further enhancements were pursued to improve the performance of the ternary system to surpass that of the single Y5 system. To achieve that, the amount of Y5 was thoroughly increased from 46 wt% to 72 wt%. The comparison of the former and latter is shown in Figure 40.

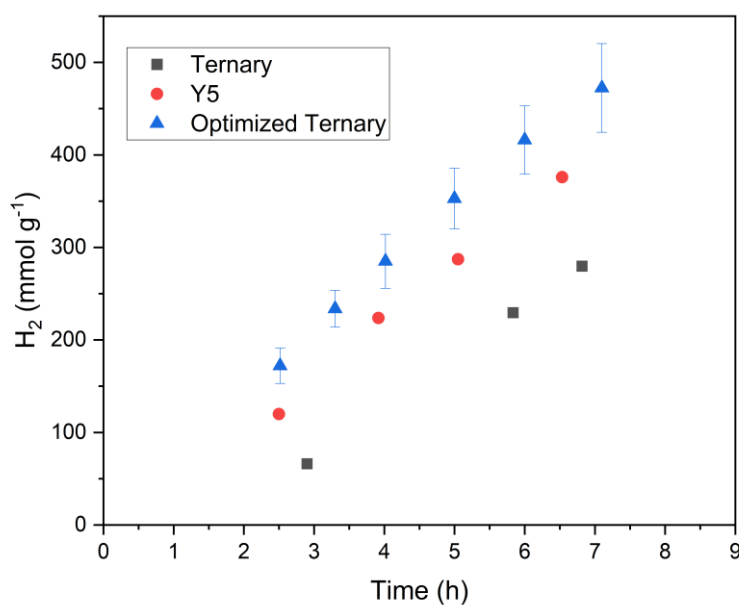


Figure 40: Comparison of optimized ternary Pdots in comparison to Y5, and ternary system before optimization.

As can be seen, the optimization increased the efficiency significantly and now outperforms the efficiency of the Y5 nanoparticle. Photocatalysis of the optimized system was performed four times. As disclaimed before, the other two were only measured once, so no error can be stated here. The optimized ternary Pdots system shows a **HER of $66.5 \pm 6.7 \text{ mmol g}^{-1} \text{ h}^{-1}$ or $1.82 \pm 0.18 \text{ mmol mL}^{-1} \text{ h}^{-1}$.**

4.3 Mechanistic Studies

In this chapter the fundamental studies, based on spectroscopy techniques, such as UV-Vis, Fluorescence and Transient Absorption Spectroscopy are shown. The findings aim to identify the roles of the different components used in the Pdots system. The background of the different spectroscopy techniques can be found in the experimental part of the work (chapter 3).

4.3.1 Possible Pathways

Firstly, the various possible pathways dependent on the energy levels of HOMO and LUMO of the three components are presented. Subsequently, the likelihood of each pathway is analyzed to determine the most probable ones. The energy diagram showing all the energy levels and band gaps of the components used in the Pdots system can be seen in Figure 41. The energy levels of the components were taken from the following sources (8, 59, 68).

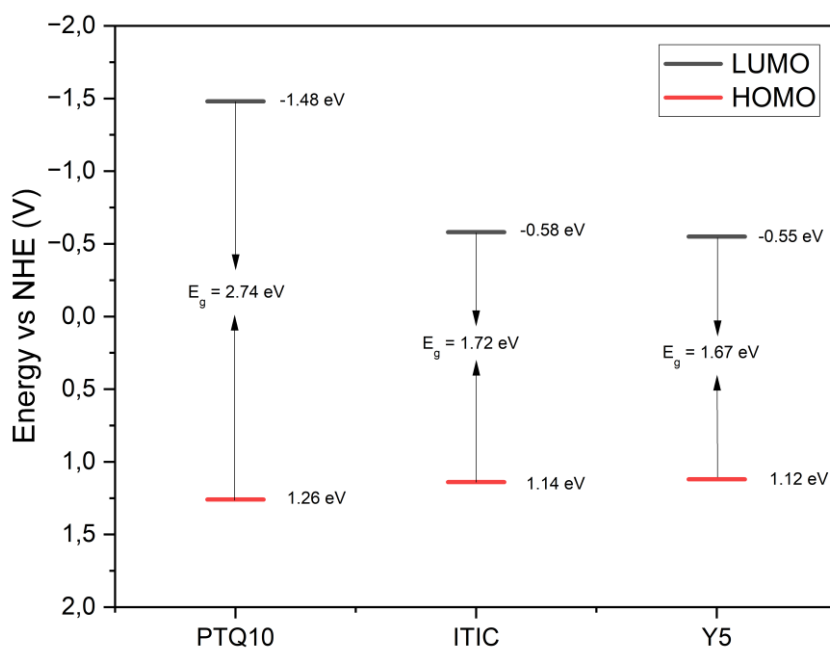


Figure 41: Energy diagram of the three components used in the Pdots system.

As discussed in sub-chapter 1.3.2 the combination of different molecules within a system enables three possible types of heterojunctions:

- Type I: Straddling Gap
- Type II: Staggered Gap
- Type III: Broken Gap

Based on this, the binary systems can be assigned to a certain type, to be able to identify the possible mechanism that can later be observed.

As can be seen in Figure 41 all binary systems show type I straddling gaps, where energy and/or charge transfer can only come from the molecule with the larger band gap. In detail this means transfer processes from PTQ10 to both ITIC and Y5, and from ITIC to Y5 can be expected.

4.3.2 Absorption and Fluorescence Spectra

As mentioned in the introduction, a major advantage of organic semiconductors in comparison to inorganic ones is the ease to tune the bandgap, so that a large portion of the sunlight can be absorbed. Since it is difficult to synthesize a polymer or molecule that can absorb in the whole visible range, one can combine different components, to complement their spectra over a larger wavelength region.

Figure 42 shows the normalized absorption (thick lines) and fluorescence (dashed lines) spectra of each component. The three components complement each other well in the region from 450 nm up to the NIR region of 850 nm. Furthermore, the emitted photons of PTQ10 and ITIC overlap perfectly with the absorption of Y5, which is vital for efficient energy transfer, as discussed in sub-chapter 1.3.2.

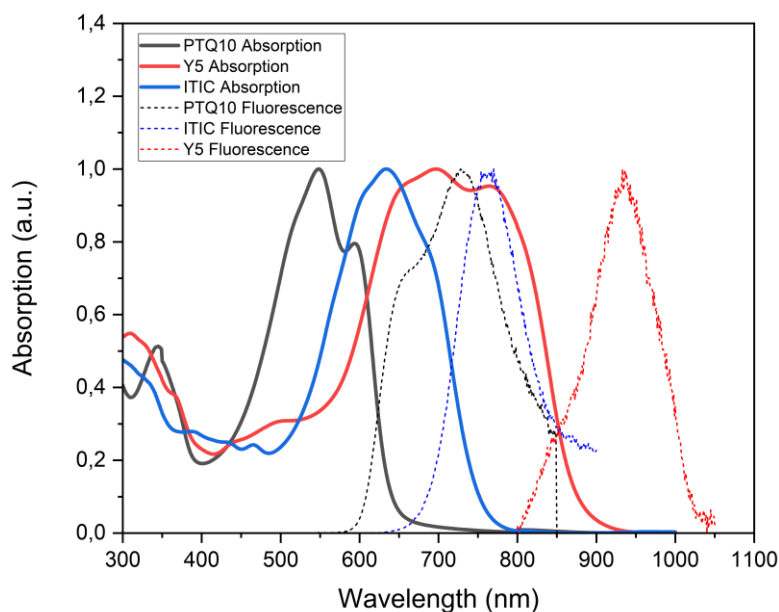


Figure 42: Normalized Absorption and Fluorescence Spectra of PTQ10 (black), ITIC (blue) and Y5 (red).

4.3.3 Quenching Experiments

Quenching describes the deactivation processes that excited molecules undergo in vicinity of other components (27). These processes can be quantitatively measured through the decrease in fluorescence emission, and they can indicate energy and/or charge transfer reactions. The description of the experimental procedure can be found in sub-chapter 3.4.1. The results are shown in Figure 43.

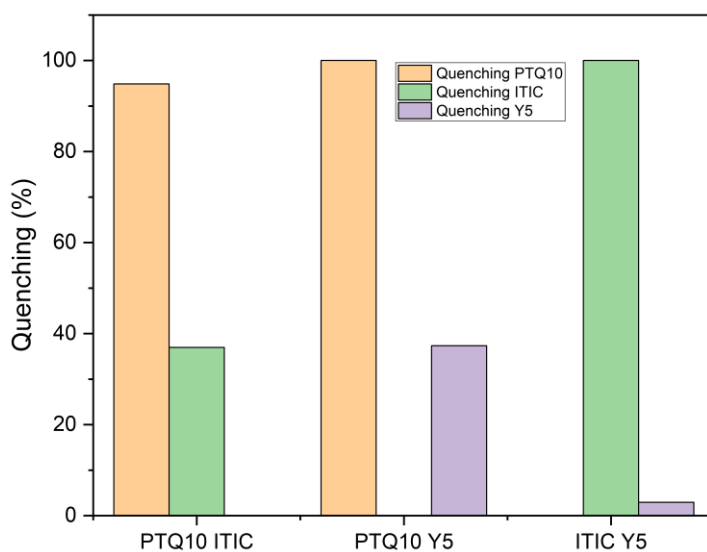


Figure 43: Quenching results of the three binary systems

As discussed before, PTQ10/ITIC can be assigned to a type I straddling gap. This would enable charge and/or energy transfer from PTQ10 to ITIC. A quenching of 95 % indicates that a majority of the excited PTQ10 molecule undergoes these transfer processes, however these quenching experiments alone cannot enable a differentiation between energy and charge transfer. A quenching of 37 % of ITIC by PTQ10 cannot be explained by transfer processes since type I gaps only allows these processes from donor PTQ10 to acceptor ITIC. The quenching could therefore come from the different chemical environment, that arises through the different morphology of ITIC in combination of PTQ10 compared to single ITIC particles. This could impact the fluorescence emission and therefore explain the quenching of ITIC in binary system with PTQ10.

Similar observations can be made for PTQ10/Y5 binary systems. In this case PTQ10 even shows quenching close to 100 % and Y5 38 %, similar to ITIC with PTQ10. Since PTQ10/Y5 is also assigned to a type I heterojunction, analogously to PTQ10/ITIC, this cannot be explained through transfer processes between the molecules, that are only expected to come from PTQ10 to Y5. Therefore, similar considerations as were made for ITIC, can be made here again, explaining the quenching through different chemical environments.

ITIC/Y5 also presents a type I straddling gap. Here ITIC is quenched to an amount close to 100 %, while Y5 shows very poor quenching of only about 2 %, which shows good resemblance with type I straddling gap theory. The strong quenching of ITIC should be from energy transfer only, since a gap between the LUMO levels of ITIC and Y5 of only 30 mV would not lead to efficient electron transfer.

For these experiments it was assumed that, at the chosen excitation wavelengths, only the desired component would get excited, while the absorption of other components can be neglected. However,

looking at Figure 42 one notices that this is not completely true for the excitation of PTQ10 with both ITIC and Y5, as well as the excitation of ITIC with Y5. Absorption of the undesired component would falsely increase the expected emission of the actual measured component and therefore to a falsely higher quenching value. However, since PTQ10 with Y5 and ITIC with Y5 showed quenching results of 100 %, an absorption of the undesired component would not have changed the fact, that the quenching exterminated the entire emission signal. Therefore, only the quenching of 94 % of PTQ10 with ITIC, might in fact be smaller, when considering a minor contribution to absorption coming from ITIC.

4.4.4 Energy and Charge Transfer Studies

As pointed out in the previous chapter, quenching indicates charge and/or energy transfer. A method to distinguish between energy and charge transfer was introduced in the experimental part of this work in chapter 3.4.2. Based on this method the binary systems PTQ10/Y5 and ITIC/Y5 were studied. The binary system PTQ10/ITIC could not be investigated with this method as the emission spectra of these components overlap too much. The results are shown in Figure 44 and Figure 45.

The absorption and excitation spectra of the binary system ITIC/Y5 overlap very well, which indicates a dominance of energy transfer, confirming the assumption from the previous sub-chapter. The excitation spectrum of PTQ10/Y5 shows a clear decrease in comparison to the absorption spectrum. This indicates a certain amount of electron transfer from PTQ10 to Y5.

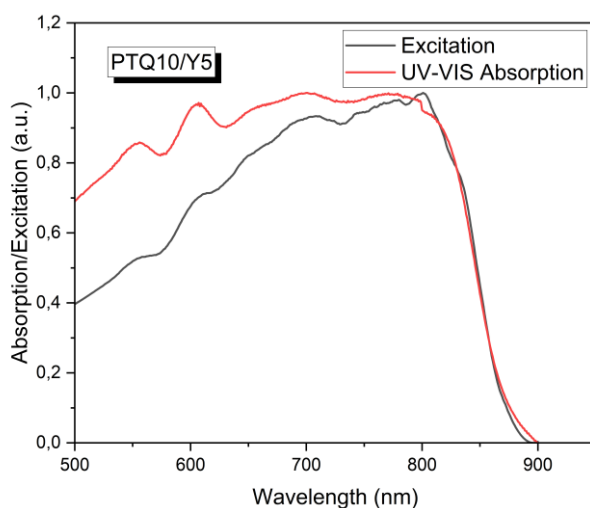


Figure 44: Absorption and Excitation Spectra of PTQ10/Y5 binary pdots

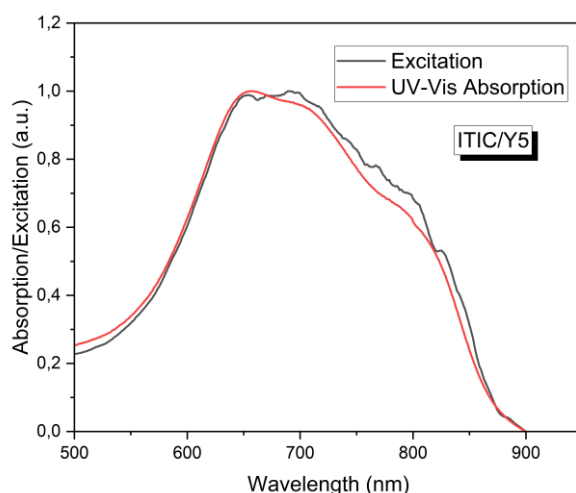


Figure 45: Absorption and Excitation Spectra of ITIC/Y5 binary pdots

A contribution of charge transfer from PTQ10 to Y5, as shown in Figure 44 is based on the assumption of nearly 100 % quenching of PTQ10 by Y5, which was shown in the previous chapter. Meanwhile, for the binary system of ITIC/Y5, shown in Figure 45, the only remaining explanation of the perfect overlap is nearly 100 % quenching of ITIC by Y5, through energy transfer. This finding is independent of the previous quenching experiments.

This method is meant to give a qualitative first impression of the possible mechanisms and is not capable to return quantitative results of the underlying processes. Therefore, the findings need to be further confirmed with TAS studies.

4.4.5 Transient Absorption Spectroscopy (TAS) Studies

Based on the previous investigations the goal of the TAS measurements is to better understand the underlying processes. The aim is to investigate the limitations to the efficiency through interaction of the different components. The measurements were aimed at investigating exciton formation and charge transfer processes. Therefore, measurements of PTQ10, binary samples and the ternary sample were performed.

Absorption Spectra of Binary Systems

The absorption spectra of the binary system help to discuss the TAS data. The normalized data is shown in Figure 46, where in each spectrum black shows the absorption of the binary systems, while red and blue indicate donor and acceptor contributions, respectively.

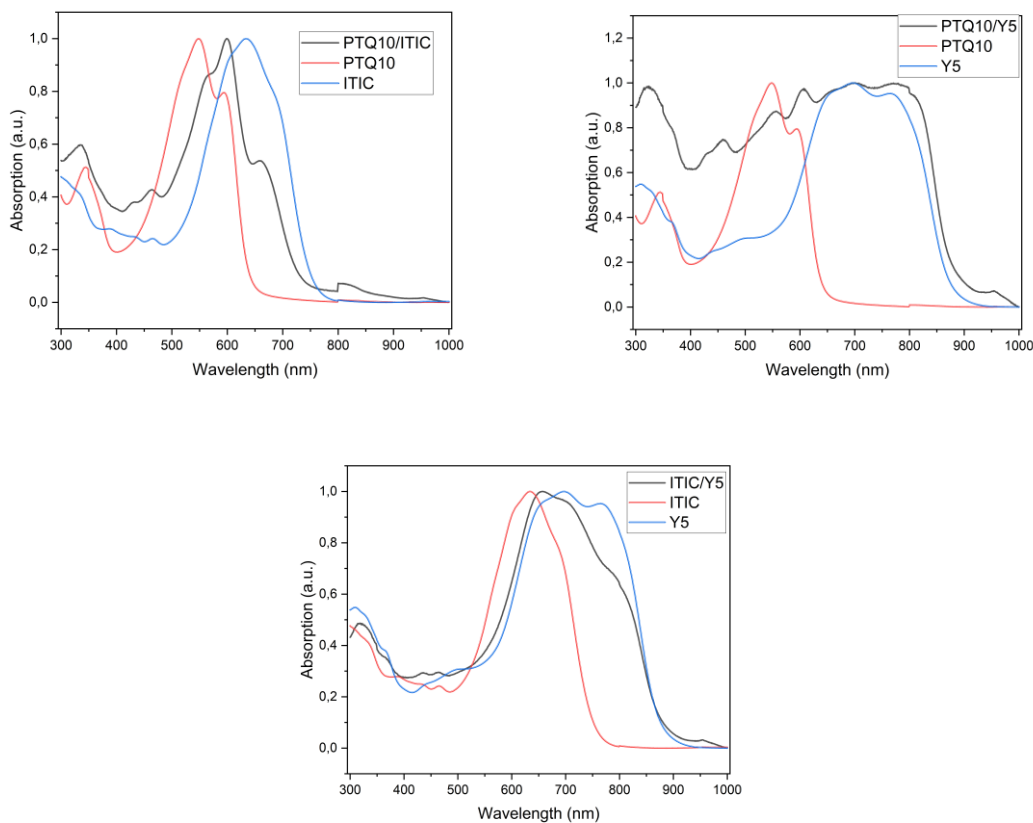


Figure 46: UV-Vis Absorption of binary systems.

Electrochemical Data

Charge Transfer can be seen in TAS measurements through emerging of product absorption peaks at wavelengths characteristic for reductive and oxidative species, respectively. To be able to compare this signal, spectroelectrochemical data is vital. The data of reduced ITIC, shown in Figure 47 was taken from Liu et al. (8) and the data of Y5, shown in Figure 48 was provided by the research group of Professor Haining Tian at Uppsala University.

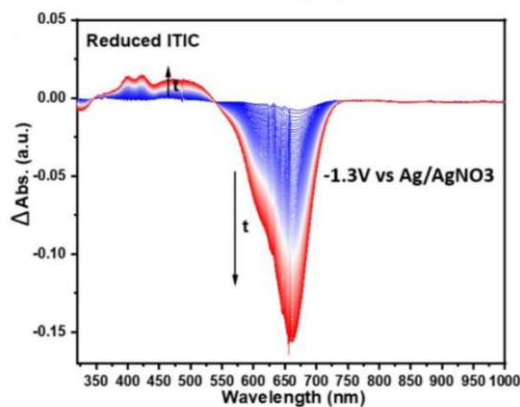


Figure 47: Spectroelectrochemical data of ITIC (8).

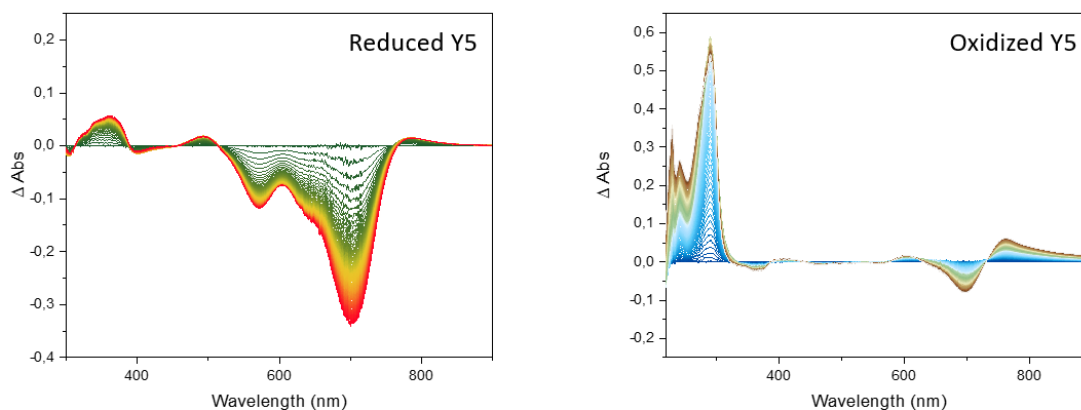


Figure 48: Spectroelectrochemical data of Y5.

PTQ10

In Figure 49 the TA spectra of PTQ10 are shown. The strong negative signal between 450 and 650 nm is the GSB of PTQ10 as it overlaps well with the absorption spectra, shown in Figure 42.

Excited state absorption (ESA) can be observed between 620 to above 750 nm, where half of it dissipates within 40 ps, but still shows some absorption even after 1 ns. The rather long-lived excited state is an indication of the good photocatalytic activity of PTQ10.

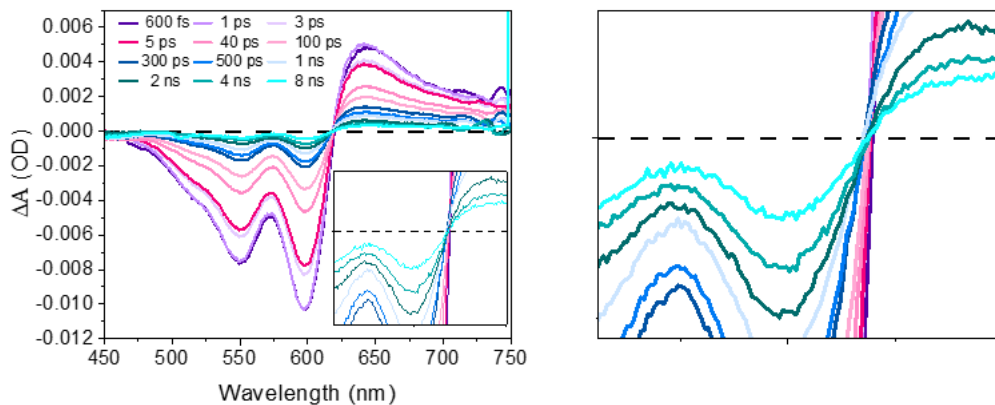


Figure 49: TAS of PTQ10 Pdots at an excitation wavelength of 510 nm.

Enlargement of the spectrum (Figure 49 left) shows an infinite persisting component. Its kinetic trace is shown in Figure 50. The global analysis returns a sum of three kinetic decays with a very fast one at 3 ps, while half of it decays in 73 ps, and a portion of 15 % shows a rather long lifetime of over 1 ns.

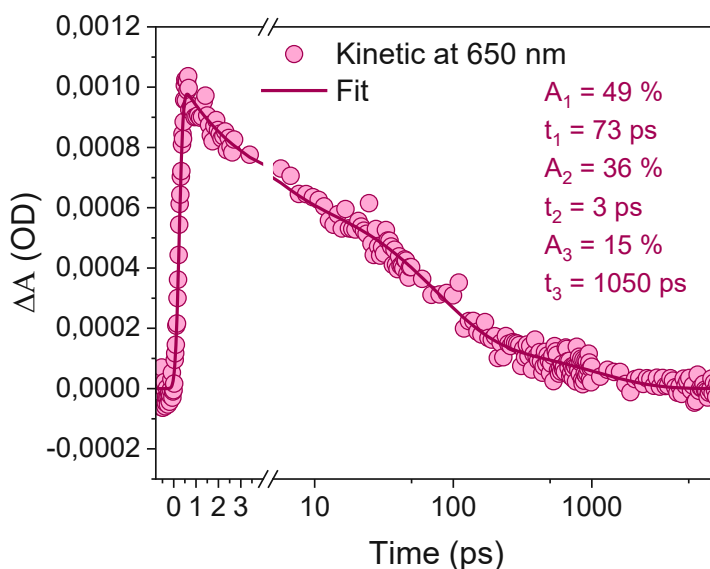


Figure 50: Kinetic trace of PTQ10 at 650 nm.

PTQ10/ITIC

As discussed before, PTQ10/ITIC is a type I straddling gap, where energy and charge transfer can occur from PTQ10 to ITIC.

Steady state studies showed very high quenching of PTQ10 with ITIC, which suggests effective charge or energy transfer. However, since the emission spectra of PTQ10 and ITIC are overlapping too strongly, no prior steady state experiments could help to differentiate between energy or charge transfer.

The TAS data of the binary system PTQ10/ITIC with a pump wavelength of 510 nm is shown in Figure 51.

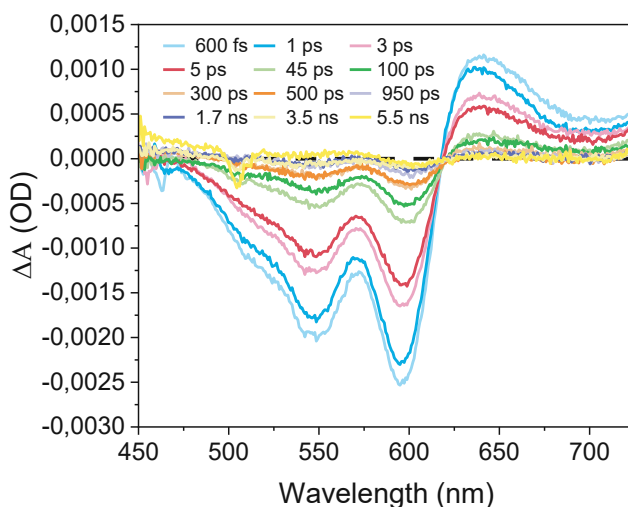


Figure 51: TAS of PTQ10/ITIC binary pdots at an excitation wavelength of 510 nm

The pump was mainly exciting PTQ10, which is why predominantly GSB of PTQ10 can be observed. However, effective energy transfer from PTQ10 to ITIC should show the emergence of GSB from ITIC, appearing between 650 and 700 nm, while GSB of PTQ10 slowly dissipates. Energy transfer might be very slow here, which is why the experiments of maximum 5 ns could have been too short to detect the transfer process, happening from PTQ10 to ITIC. To confirm this, further measurements need to be performed aiming for longer time frames.

The spectroelectrochemical data in Figure 47 shows that ESA of reduced ITIC would be expected around 500 nm. Unfortunately, this can not be confirmed as GSB of PTQ10 overlaps with ESA of reduced ITIC.

The normalized kinetics of ESA between 620 and 750 nm were compared with normalized ESA kinetics of single PTQ10 nanoparticles in Figure 52. The faster decay of the binary system probably indicates the presence of energy or charge transfer from PTQ10 to ITIC, as it provides another decay path and therefore accelerates the decay of the excited PTQ10. This would confirm the assumptions from the steady state quenching experiments. However, as mentioned before, neither energy nor electron transfer could have been identified in the TA spectra.

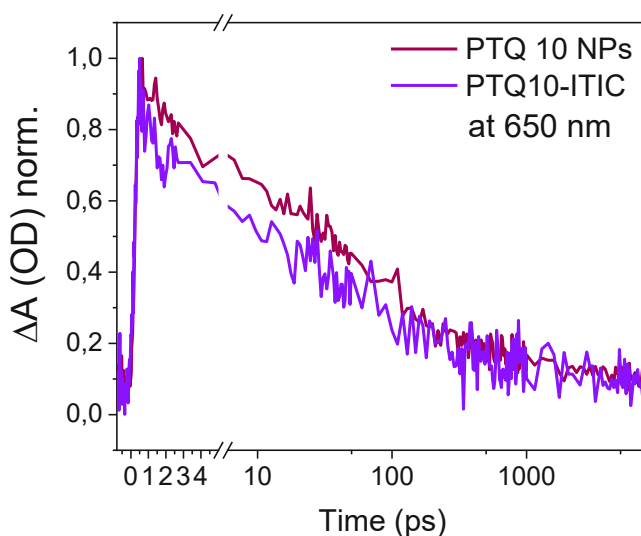


Figure 52: Normalized kinetic traces of PTQ10 pdots (red) and PTQ10/ITIC binary pdots (blue) at an absorption of 650 nm

The kinetic decay of the GSB is shown in Figure 53. Global analysis returns a sum of three decays with lifetimes of 42 % of 33 ps, 37 % of 1.5 ps and 22 % of 346 ps.

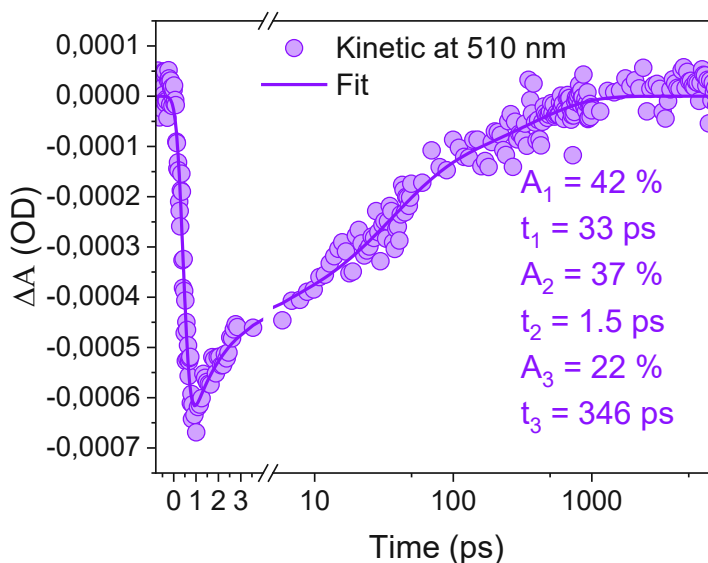


Figure 53: Kinetic trace of GSB of PTQ10/ITIC pdots at 510 nm

To summarize, the kinetics data indicated the quenching of PTQ10 by ITIC through energy and/or charge transfer, which is consistent with the steady state quenching data, however excited or reduced ITIC could not have been identified. Excited ITIC could be further investigated by extending the experimental time frame, to over 10 ns, to observe possible slow energy transfer. However, reduced ITIC, would be difficult to identify with TAS, since a dominant GSB of PTQ10 overlaps with a rather weak ESA signal of reduced ITIC.

PTQ10/Y5

Analogously to PTQ10/ITIC, steady state experiments also showed high quenching of PTQ10 in presence of Y5. The comparison of excitation and absorption spectra suggested contribution of charge transfer. The TAS data of the binary system PTQ10/Y5 at a pump wavelength of 510 nm (PTQ10 absorption) is shown in Figure 54. Again, the GSB of PTQ10 can be seen between 470 and 650 nm, as well as ESA of PTQ10 at 620 to 750 nm.

Again, for efficient energy transfer from PTQ10 to Y5, one would expect GSB of Y5, at wavelengths over 650 nm. However, no GSB can be identified. Slow energy transfer at times longer than 10 ns could again explain why no energy transfer can be observed. Furthermore, the binary PTQ10/Y5 Pdots have a mass ratio of 1:5.6. This results in a rather poor absorption of the less represented PTQ10, seen in Figure 54. For further measurements either the mass ratio or the overall concentration of the sample should be increased to enable better absorption.

The spectroelectrochemical data of Y5 in Figure 48 shows possible signals of reduced and oxidized Y5 either below 400 nm or above 750 nm, which unfortunately both lie outside the investigated spectral region and could therefore not be detected.

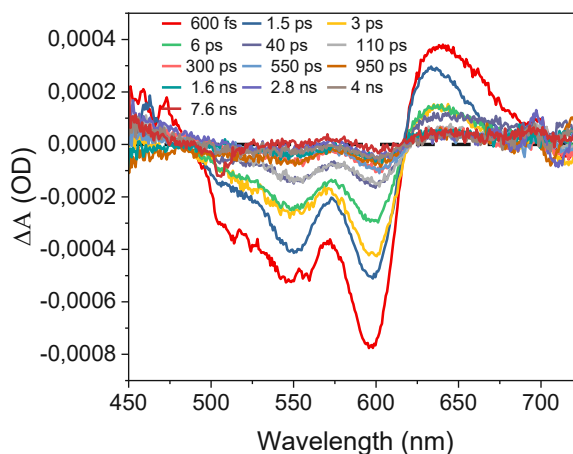


Figure 54: TAS of PTQ10/Y5 at an excitation wavelength of 510 nm

To summarize, due to the low concentration of PTQ10 in the binary system the TAS data could not confirm energy or charge transfer processes. For further studies the overall concentration of the sample needs to be increased, and the spectral region should be enlarged to below 400 nm to be able to detect ESA of reduced Y5.

ITIC/Y5

Figure 55 shows the TAS data of the binary system ITIC/Y5. The energy/charge transfer studies in the previous chapter predicted 100 % energy transfer from ITIC to Y5, so no formation of reduced species should be observed.

Again, the mass ratio of ITIC:Y5 of 1:4.6 leads to low absorption of the donor molecule ITIC. Furthermore, the overall absorption of this binary system is not high at the pump wavelength of 510 nm, as shown in Figure 46. This is why only small GSB signals of ITIC and Y5 can be observed in the TAS data shown in Figure 55. In general, the similar absorption profiles of ITIC and Y5 make it difficult to investigate transfer processes between them, which might also limit future attempts to study them.

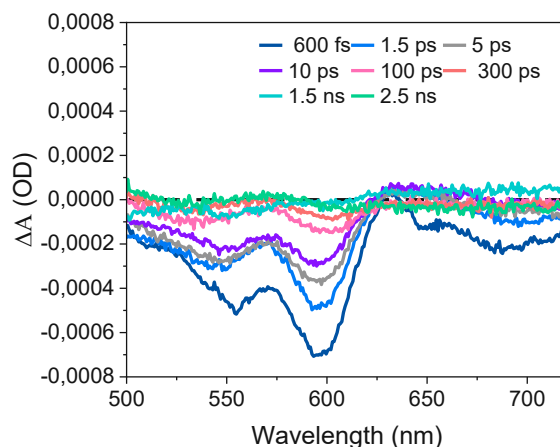


Figure 55: TAS of ITIC/Y5 at an excitation wavelength of 510 nm

Ternary (PTQ10/ITIC/Y5)

The TAS data of the ternary system at a pump wavelength of 510 nm is shown in Figure 56 and the data with a pump wavelength of 590 nm is shown in Figure 57. An excitation wavelength of 510 nm should predominantly excite PTQ10, while an excitation wavelength of 590 nm can partly be absorbed by all components.

The excitation at 510 nm shows the characteristic GSB of PTQ10 like in the previous examples. The pump laser at 590 nm induces a stronger GSB at 600 nm, where both PTQ10 and ITIC absorb, while the peak at 550 nm only comes from PTQ10, which is now less dominant. Both show ESA at 620 to 750 nm, and again an infinite component remains even at 8 ns.

Again, the formation of reduced species cannot be identified, since they either lie outside the obtained spectral range or they overlap with a predominant GSB.

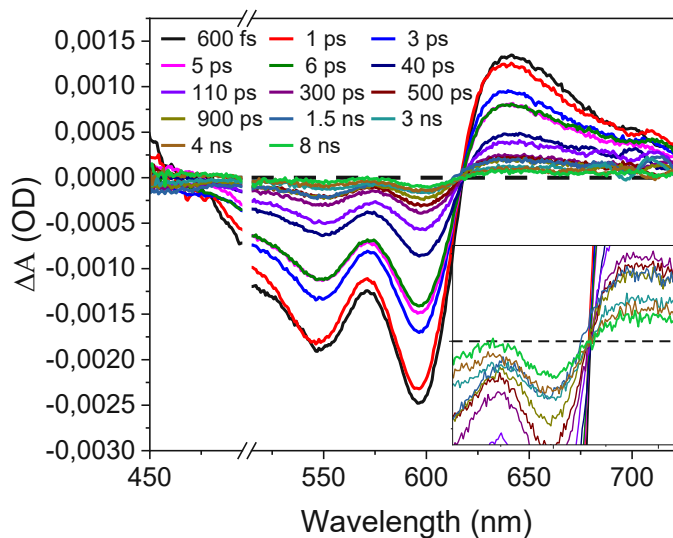


Figure 56: TAS spectra of ternary system at an excitation wavelength of 510 nm

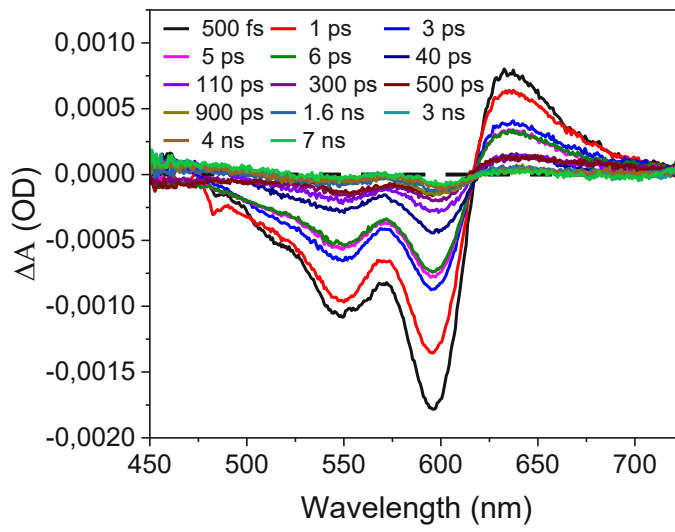


Figure 57: TAS spectra of ternary system at an excitation wavelength of 590 nm

5 Conclusion & Outlook

The research of organic catalysts for water splitting reactions is still in an early stage. However, the fast progress in the past decade has shown the vast potential in this field. Studying new efficient systems is key to a better fundamental understanding of the underlying processes. These findings will help to further advance this method and establish it as an effective way for green hydrogen production.

In this work a new ternary system with the components PTQ10, ITIC and Y5 was presented, which showed a HER of $66.5 \text{ mmol g}^{-1} \text{ h}^{-1}$ or $1.82 \text{ mL g}^{-1} \text{ h}^{-1}$. The system was also tested on the efficiency of its binary and single subgroups. A remarkable result was observed for single Y5 Pdots, which showed an efficiency close to the ternary system. This indicated that efficient Pdots without heterojunctions can be produced. However, the extraordinary efficiency of Y5 needs to be further investigated, to understand its full potential.

Quenching of the components in vicinity of other components was investigated through steady state spectroscopy on binary Pdots. This showed highly effective quenching of PTQ10 with both ITIC and Y5, which indicated efficient energy and/or charge transfer. Furthermore, steady state experiments with the binary system PTQ10 and Y5 indicated a combination of charge and energy transfer. The same combination was suggested for PTQ10 with ITIC. The comparison of normalized kinetic data between single PTQ10 and binary PTQ10/ITIC, suggested the presence of energy and/or charge transfer, which was also indicated by the quenching experiments. However, this could not have been completely confirmed with the TAS data.

The utilization of multicomponent Pdots offers two distinct advantages for photocatalytic applications. Firstly, they exhibit complementary absorption spectra, facilitating the maximization of the quantum yield from incoming photons. Secondly, the introduction of heterojunctions reduces recombination rates by facilitating charge transfer, resulting in the formation of long-lived reduced and oxidized states that can initiate further redox reactions.

In this work, it was demonstrated that individual components within a multicomponent system do not need to be efficient photocatalysts by themselves to enhance the overall efficiency. This was exemplified through the investigation of PTQ10. When tested as single PTQ10 Pdots in photocatalytic experiments, the efficiency was found to be poor. However, the inclusion of PTQ10 in the ternary system PTQ10/ITIC/Y5 significantly improved the overall efficiency compared to the binary Pdots system ITIC/Y5. This improvement can be attributed to PTQ10's absorption of light at lower wavelengths, thereby increasing the quantum yield of the entire system.

Moreover, steady-state spectroscopy experiments provided valuable insights into the efficient energy transfer from PTQ10 to ITIC and Y5 within the multicomponent system, confirming the mechanism responsible for the enhanced photocatalytic efficiency.

Even though some clear conclusions could be drawn by the methods presented in this work, there is still great potential in further investigation of this system. The TAS experiments were performed without photodeposited Pt. The next step is to investigate the transfer mechanism between the different components to Pt, which is also vital for the efficiency. Liu et al. have studied a similar system with and without Pt (8). The TAS data showed a longer lived GSB, indicating that Pt helps reduce charge recombination. Furthermore, the exact structure and its impact on the efficiency could be studied for example with Cryo-TEM. Ultimately, achieving optimization will likely depend on the continuous advancement of organic photocatalysts, as well as their right implementation within an interacting system.

Appendix

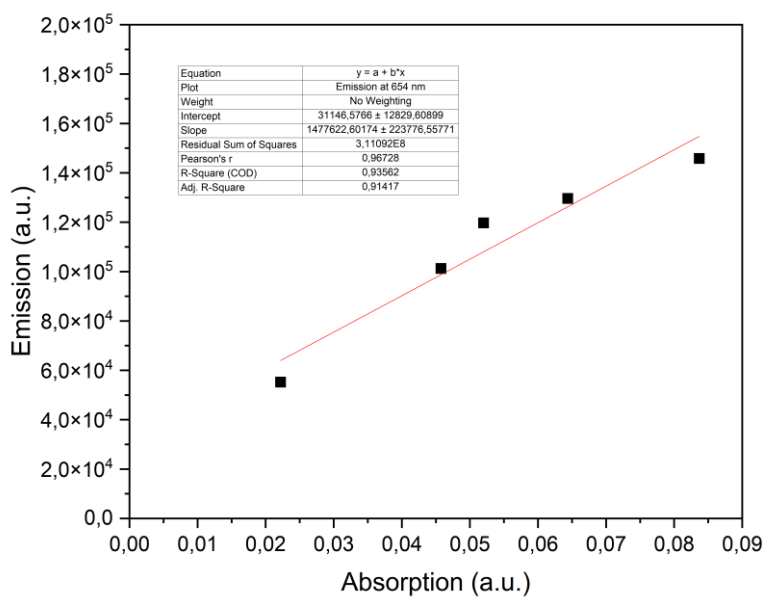


Figure 58: Emission vs Absorption calibration curve of PTQ10 for emission wavelengths at 654 nm

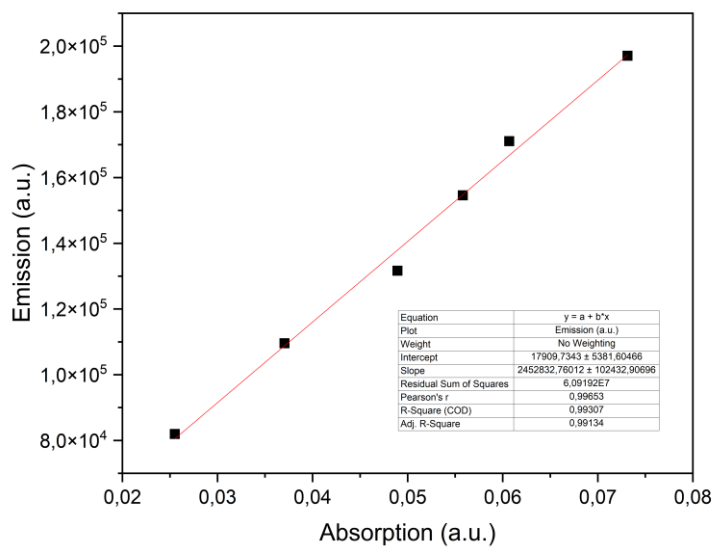


Figure 59: Emission vs Absorption calibration curve of ITIC at 591 nm

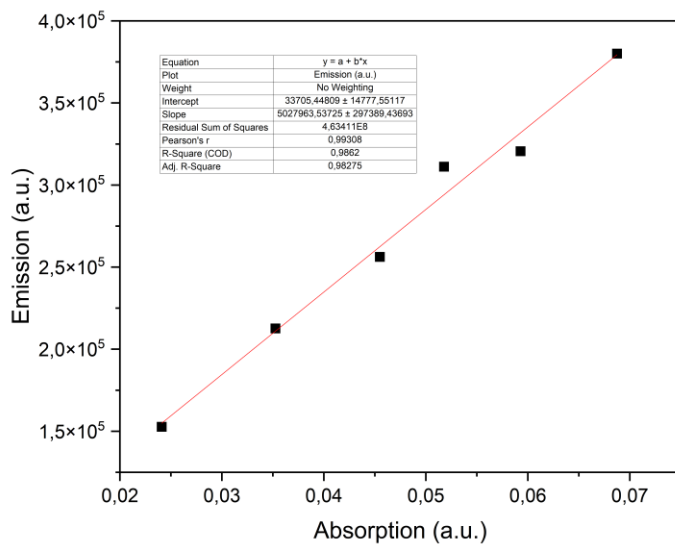


Figure 60: Emission vs Absorption calibration curve of ITIC at 676 nm

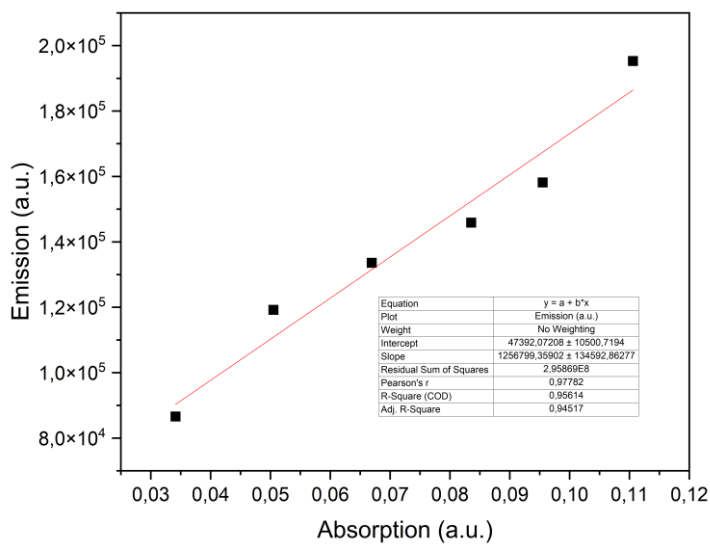


Figure 61: Emission vs Absorption calibration curve of Y5

References

1. Di Napoli C, McGushin A, Romanello M, Ayeb-Karlsson S, Cai W, Chambers J, et al. Tracking the impacts of climate change on human health via indicators: lessons from the Lancet Countdown. *BMC public health*. 2022;22(1):1-8.
2. Shukla PR, Skea J, Calvo Buendia E, Masson-Delmotte V, Pörtner HO, Roberts D, et al. IPCC, 2019: Climate Change and Land: an IPCC special report on climate change, desertification, land degradation, sustainable land management, food security, and greenhouse gas fluxes in terrestrial ecosystems. 2019.
3. Newell R, Raimi D, Aldana G. Global energy outlook 2019: the next generation of energy. *Resources for the Future*. 2019;1:8-19.
4. Lutz W, KC S. Dimensions of global population projections: what do we know about future population trends and structures? *Philosophical Transactions of the Royal Society B: Biological Sciences*. 2010;365(1554):2779-91.
5. Koochi-Fayegh S, Rosen MA. A review of energy storage types, applications and recent developments. *Journal of Energy Storage*. 2020;27:101047.
6. Lubitz W, Tumas W. Hydrogen: an overview. *Chemical reviews*. 2007;107(10):3900-3.
7. da Silva Veras T, Mozer TS, da Silva César A. Hydrogen: trends, production and characterization of the main process worldwide. *International journal of hydrogen energy*. 2017;42(4):2018-33.
8. Liu A, Gedda L, Axelsson M, Pavliuk M, Edwards K, Hammarström L, et al. Panchromatic ternary polymer dots involving sub-picosecond energy and charge transfer for efficient and stable photocatalytic hydrogen evolution. *Journal of the American Chemical Society*. 2021;143(7):2875-85.
9. Rahman M, Tian H, Edvinsson T. Revisiting the limiting factors for overall water-splitting on organic photocatalysts. *Angewandte Chemie*. 2020;132(38):16418-33.
10. Balzani V, Armaroli N. *Energy for a sustainable world: from the oil age to a sun-powered future*: John Wiley & Sons; 2010.
11. Abbasi T, Abbasi S. Biomass energy and the environmental impacts associated with its production and utilization. *Renewable and sustainable energy reviews*. 2010;14(3):919-37.
12. Tursi A. A review on biomass: importance, chemistry, classification, and conversion. *Biofuel Research Journal*. 2019;6(2):962.
13. Tarhan C, Çil MA. A study on hydrogen, the clean energy of the future: Hydrogen storage methods. *Journal of Energy Storage*. 2021;40:102676.
14. Zhang Y-h, Jia Z-c, Yuan Z-m, Yang T, Qi Y, Zhao D-l. Development and application of hydrogen storage. *Journal of Iron and Steel Research International*. 2015;22(9):757-70.
15. Midilli A, Ay M, Dincer I, Rosen MA. On hydrogen and hydrogen energy strategies: I: current status and needs. *Renewable and sustainable energy reviews*. 2005;9(3):255-71.
16. Abe JO, Popoola A, Ajenifuja E, Popoola OM. Hydrogen energy, economy and storage: Review and recommendation. *International journal of hydrogen energy*. 2019;44(29):15072-86.
17. Ley MB, Jepsen LH, Lee Y-S, Cho YW, Von Colbe JMB, Dornheim M, et al. Complex hydrides for hydrogen storage—new perspectives. *Materials Today*. 2014;17(3):122-8.
18. Rusman N, Dahari M. A review on the current progress of metal hydrides material for solid-state hydrogen storage applications. *International Journal of Hydrogen Energy*. 2016;41(28):12108-26.
19. Ho SH, Rahman MM. Three-dimensional analysis for liquid hydrogen in a cryogenic storage tank with heat pipe–pump system. *Cryogenics*. 2008;48(1-2):31-41.
20. Molname M, Schroeder V. Hazardous properties of hydrogen and hydrogen containing fuel gases. *Process Safety and Environmental Protection*. 2019;130:1-5.
21. Najjar YS. Hydrogen safety: The road toward green technology. *International Journal of Hydrogen Energy*. 2013;38(25):10716-28.
22. XIE L. Experimental study on minimum ignition energy of diesel-air cloud. *Chinese Journal of High Pressure Physics*. 2015;29(2):149-54.

23. Swai MRA, R.R.; Pappas, J.M.; Experimental hydrogen-fuelled automotive engine design project. Prepared for US Dept of energy. 1983.
24. Simkin AJ. Genetic engineering for global food security: Photosynthesis and biofortification. *Plants*. 2019;8(12):586.
25. Redfield A. *Advances in Magnetic and Optical Resonance*, Vol. 1. Academic Press Inc; 1965.
26. Fassioli F, Dinshaw R, Arpin PC, Scholes GD. Photosynthetic light harvesting: excitons and coherence. *Journal of The Royal Society Interface*. 2014;11(92):20130901.
27. Balzani V, Ceroni P, Juris A. *Photochemistry and photophysics: concepts, research, applications*: John Wiley & Sons; 2014.
28. Fujishima A, Honda K. Electrochemical photolysis of water at a semiconductor electrode. *nature*. 1972;238(5358):37-8.
29. Marschall R. Semiconductor composites: strategies for enhancing charge carrier separation to improve photocatalytic activity. *Advanced Functional Materials*. 2014;24(17):2421-40.
30. Khan MA, Woo SI, Yang O-B. Hydrothermally stabilized Fe (III) doped titania active under visible light for water splitting reaction. *International Journal of Hydrogen Energy*. 2008;33(20):5345-51.
31. Shi R, Ye HF, Liang F, Wang Z, Li K, Weng Y, et al. Interstitial P-doped CdS with long-lived photogenerated electrons for photocatalytic water splitting without sacrificial agents. *Advanced Materials*. 2018;30(6):1705941.
32. Yanagida S, Kabumoto A, Mizumoto K, Pac C, Yoshino K. Poly (p-phenylene)-catalysed photoreduction of water to hydrogen. *Journal of the Chemical Society, Chemical Communications*. 1985(8):474-5.
33. Wang X, Maeda K, Thomas A, Takanabe K, Xin G, Carlsson JM, et al. A metal-free polymeric photocatalyst for hydrogen production from water under visible light. *Nature materials*. 2009;8(1):76-80.
34. Sprick RS, Jiang J-X, Bonillo B, Ren S, Ratvijitvech T, Guiglion P, et al. Tunable organic photocatalysts for visible-light-driven hydrogen evolution. *Journal of the American Chemical Society*. 2015;137(9):3265-70.
35. Wang L, Fernández-Terán R, Zhang L, Fernandes DL, Tian L, Chen H, et al. Organic polymer dots as photocatalysts for visible light-driven hydrogen generation. *Angewandte Chemie International Edition*. 2016;55(40):12306-10.
36. Vitale SA, Katz JL. Liquid droplet dispersions formed by homogeneous liquid– liquid nucleation: “The Ouzo effect”. *Langmuir*. 2003;19(10):4105-10.
37. Lepeltier E, Bourgaux C, Couvreur P. Nanoprecipitation and the “Ouzo effect”: Application to drug delivery devices. *Advanced drug delivery reviews*. 2014;71:86-97.
38. Jun H, Fabienne T, Florent M, Coulon P-E, Nicolas M, Olivier S. Understanding of the size control of biocompatible gold nanoparticles in millifluidic channels. *Langmuir*. 2012;28(45):15966-74.
39. Watzky MA, Finke RG. Transition metal nanocluster formation kinetic and mechanistic studies. A new mechanism when hydrogen is the reductant: slow, continuous nucleation and fast autocatalytic surface growth. *Journal of the American Chemical Society*. 1997;119(43):10382-400.
40. Lifschitz I, Slyozov V. The kinetics of precipitation from supersaturated solid solutions. *J Phys Chem Solids*. 1961;19(1/2):35-50.
41. Wagner C. Theorie der alterung von niederschlägen durch umlösen (Ostwald-reifung). *Zeitschrift für Elektrochemie, Berichte der Bunsengesellschaft für physikalische Chemie*. 1961;65(7-8):581-91.
42. Liu Y, Kathan K, Saad W, Prud’homme RK. Ostwald ripening of β -carotene nanoparticles. *Physical Review Letters*. 2007;98(3):036102.
43. Fessi H, Puisieux F, Devissaguet JP, Ammoury N, Benita S. Nanocapsule formation by interfacial polymer deposition following solvent displacement. *International journal of pharmaceutics*. 1989;55(1):R1-R4.
44. Bilati U, Allémann E, Doelker E. Development of a nanoprecipitation method intended for the entrapment of hydrophilic drugs into nanoparticles. *European Journal of Pharmaceutical Sciences*. 2005;24(1):67-75.

45. Pavliuk MV, Wrede S, Liu A, Brnovic A, Wang S, Axelsson M, et al. Preparation, characterization, evaluation and mechanistic study of organic polymer nano-photocatalysts for solar fuel production. *Chemical Society Reviews*. 2022.
46. Clarke TM, Durrant JR. Charge photogeneration in organic solar cells. *Chemical reviews*. 2010;110(11):6736-67.
47. Gledhill SE, Scott B, Gregg BA. Organic and nano-structured composite photovoltaics: An overview. *Journal of Materials Research*. 2005;20(12):3167-79.
48. Lu L, Zheng T, Wu Q, Schneider AM, Zhao D, Yu L. Recent advances in bulk heterojunction polymer solar cells. *Chemical reviews*. 2015;115(23):12666-731.
49. Bruno A, Reynolds L, Dyer-Smith C, Nelson J, Haque S. Determining the exciton diffusion length in a polyfluorene from ultrafast fluorescence measurements of polymer/fullerene blend films. *The Journal of Physical Chemistry C*. 2013;117(39):19832-8.
50. Kosco J, Gonzalez-Carrero S, Howells CT, Fei T, Dong Y, Sougrat R, et al. Generation of long-lived charges in organic semiconductor heterojunction nanoparticles for efficient photocatalytic hydrogen evolution. *Nature Energy*. 2022;7(4):340-51.
51. Sachs M, Cha H, Kosco J, Aitchison CM, Francàs L, Corby S, et al. Tracking charge transfer to residual metal clusters in conjugated polymers for photocatalytic hydrogen evolution. *Journal of the American Chemical Society*. 2020;142(34):14574-87.
52. Förster T. 10th Spiers Memorial Lecture. Transfer mechanisms of electronic excitation. *Discussions of the Faraday Society*. 1959;27:7-17.
53. Barigelletti F, Flamigni L. Photoactive molecular wires based on metal complexes. *Chemical Society Reviews*. 2000;29(1):1-12.
54. Dexter DL. A theory of sensitized luminescence in solids. *The journal of chemical physics*. 1953;21(5):836-50.
55. Marcus RA. Chemical and electrochemical electron-transfer theory. *Annual review of physical chemistry*. 1964;15(1):155-96.
56. Marcus RA, Sutin N. Electron transfers in chemistry and biology. *Biochimica et Biophysica Acta (BBA)-Reviews on Bioenergetics*. 1985;811(3):265-322.
57. Yang Y, Li D, Cai J, Wang H, Guo C, Wen S, et al. Enhanced Photocatalytic Hydrogen Evolution from Organic Ternary Heterojunction Nanoparticles Featuring a Compact Alloy-Like Phase. *Advanced Functional Materials*. 2023;33(10):2209643.
58. Jeong J-E, Uddin MA, Ryu HS, Kim H-C, Kang M, Joung JF, et al. Green-, red-, and near-infrared-emitting polymer dot probes for simultaneous multicolor cell imaging with a single excitation wavelength. *Chemistry of Materials*. 2020;32(15):6685-96.
59. Kong X, Zhang J, Meng L, Sun C, Qin S, Zhu C, et al. 18.55% Efficiency polymer solar cells based on a small molecule acceptor with alkylthienyl outer side chains and a low-cost polymer donor PTQ10. *CCS Chemistry*. 2023;5(4):841-50.
60. Wen G, Hu R, Su X, Chen Z, Zhang C, Peng J, et al. Excited-state properties of Y-series small molecule semiconductors. *Dyes and Pigments*. 2021;192:109431.
61. Harding S. *Protein Hydrodynamics. Protein: a comprehensive treatise*. JAI Press, Greenwich; 1999.
62. Stetefeld J, McKenna SA, Patel TR. *Dynamic light scattering: a practical guide and applications in biomedical sciences*. *Biophysical reviews*. 2016;8:409-27.
63. Pavia DL, Lampman GM, Kriz GS, Vyvyan JA. *Introduction to spectroscopy*: Cengage learning; 2014.
64. Albrecht C, Joseph R, Lakowicz: *Principles of fluorescence spectroscopy*. Springer; 2008.
65. Berera R, van Grondelle R, Kennis JT. Ultrafast transient absorption spectroscopy: principles and application to photosynthetic systems. *Photosynthesis research*. 2009;101:105-18.
66. Ruckebusch C, Sliwa M, Pernot Pd, De Juan A, Tauler R. Comprehensive data analysis of femtosecond transient absorption spectra: A review. *Journal of Photochemistry and Photobiology C: Photochemistry Reviews*. 2012;13(1):1-27.
67. Bonneau R, Wirz J, Zuberbuhler A. *Methods for the analysis of transient absorbance data (Technical Report)*. *Pure and Applied chemistry*. 1997;69(5):979-92.

68. Fan Q, An Q, Lin Y, Xia Y, Li Q, Zhang M, et al. Over 14% efficiency all-polymer solar cells enabled by a low bandgap polymer acceptor with low energy loss and efficient charge separation. *Energy & Environmental Science*. 2020;13(12):5017-27.